Cell Cycle Constraints and Environmental Control of Local DNA Hypomethylation in α-Proteobacteria

Short Title: Control of DNA Hypomethylation in α-Proteobacteria

Silvia Ardissone[1]*, Peter Redder[1#a], Giancarlo Russo[2], Antonio Frandi[1,#b], Coralie Fumeaux[1, #c],

Andrea Patrignani[2], Ralph Schlapbach[2], Laurent Falquet[3] and Patrick H. Viollier[1]*

[1] Department of Microbiology and Molecular Medicine, Institute of Genetics & Genomics in Geneva (iGE3), Faculty of Medicine, University of Geneva, Geneva, Switzerland.

[2] Functional Genomics Center Zurich, ETH/University of Zürich, Zürich, Switzerland.

[3] Biochemistry Unit, Dept. of Biology, University of Fribourg and Swiss Institute of Bioinformatics, Fribourg, Switzerland.

[#a] Current address: LMGM, Centre de Biologie Intégrative, Université Paul Sabatier, Toulouse, France.

[#b] Current address: Department of Fundamental Microbiology, University of Lausanne, Lausanne, Switzerland.

[#c] Current address: Department of Microbiology and Immunology, Harvard Medical School, Boston, MA, 02115, USA.

* Corresponding authors

Silvia.Ardissone@unige.ch (SA)

Patrick.Viollier@unige.ch (PV)

Abstract

26

27   Heritable DNA methylation imprints are ubiquitous and underlie genetic variability from bacteria to

28   humans. In microbial genomes, DNA methylation has been implicated in gene transcription, DNA

29   replication and repair, nucleoid segregation, transposition and virulence of pathogenic strains. Despite

30   the importance of local (hypo)methylation at specific loci, how and when these patterns are

31   established during the cell cycle remains poorly characterized. Taking advantage of the small genomes

32   and the synchronizability of α-proteobacteria, we discovered that conserved determinants of the cell

33   cycle transcriptional circuitry establish specific hypomethylation patterns in the cell cycle model

34   system *Caulobacter crescentus*. We used genome-wide methyl-N6-adenine (m6A-) analyses by

35   restriction-enzyme-cleavage sequencing (REC-Seq) and single-molecule real-time (SMRT)

36   sequencing to show that MucR, a transcriptional regulator that represses virulence and cell cycle genes

37   in S-phase but no longer in G1-phase, occludes 5'-GANTC-3' sequence motifs that are methylated by

38   the DNA adenine methyltransferase CcrM. Constitutive expression of CcrM or heterologous

39   methylases in at least two different α-proteobacteria homogenizes m6A patterns even when MucR is

40   present and affects promoter activity. Environmental stress (phosphate limitation) can override and

41   reconfigure local hypomethylation patterns imposed by the cell cycle circuitry that dictate when and

42   where local hypomethylation is instated.

43

Author Summary

45   DNA methylation is the post-replicative addition of a methyl group to a base by a

46   methyltransferase that recognise a specific sequence, and represents an epigenetic regulatory

47   mechanism in both eukaryotes and prokaryotes. In microbial genomes, DNA methylation has been

48   implicated in gene transcription, DNA replication and repair, nucleoid segregation, transposition and

49   virulence of pathogenic strains. CcrM is a conserved, cell cycle regulated adenine methyltransferase

50   that methylates GANTC sites in α-proteobacteria. N^6-methyl-adenine (m6A) patterns generated by

51 CcrM can change the affinity of a given DNA-binding protein for its target sequence, and therefore

52 affect gene expression. Here, we combine restriction enzyme cleavage-deep sequencing (REC-Seq)

53 with SMRT sequencing to identify hypomethylated 5'-GANTC-3' (GANTCs) in α-proteobacterial

54 genomes instated by conserved cell cycle factors. By comparing SMRT and REC-Seq data with

55 chromatin immunoprecipitation-deep sequencing data (ChIP-Seq) we show that a conserved

56 transcriptional regulator, MucR, induces local hypomethylation patterns by occluding GANTCs to the

57 CcrM methylase and we provide evidence that this competition occurs during S-phase, but not in G1-

58 phase cells. Furthermore, we find that environmental signals (such as phosphate depletion) are

59 superimposed to the cell cycle control mechanism and can override the specific hypomethylation

60 pattern imposed by the cell cycle transcriptional circuitry.

61

Keywords

62

63 REC-Seq; SMRT sequencing; hypomethylation; adenine methylation; CcrM; MucR; α-proteobacteria;

64 *Caulobacter crescentus*; *Sinorhizobium meliloti*; phosphate limitation

65

Introduction

DNA methylation is a conserved epigenetic modification that occurs from bacteria to humans and is implicated in control of transcription, DNA replication/repair, innate immunity and pathogenesis [1, 2]. Originally described as a mechanism that protects bacteria from invading foreign (viral) DNA [3], methyl-N6-adenine (m6A) modifications are thought to direct infrequent and stochastic phenotypic heterogeneity in bacterial cells [4, 5] and were recently implicated in transcriptional control of lower eukaryotic genomes [4, 5] and silencing in mouse embryonic stem cells [6-8].

How local changes in methylation are instated during the cell cycle remains poorly explored, even in γ-proteobacteria such as *Escherichia coli* and *Salmonella enterica*, as cell cycle studies on cell populations are cumbersome and require genetic manipulation [9]. Moreover, the replication regulator SeqA that controls the methylation state by preferentially binding hemi-methylated sequences is only encoded in γ-proteobacteria, suggesting that other mechanisms are likely operational in other systems [9, 10]. Model systems in which cell populations can be synchronized without genetic intervention are best suited to illuminate the interplay between methylation and cell cycle [11, 12]. The fresh-water bacterium *Caulobacter crescentus* and more recently the plant symbiont *Sinorhizobium meliloti* that reside in distinct environmental niches are such cell cycle model systems [13]. Akin to other α-proteobacteria, *C. crescentus* and *S. meliloti* divide asymmetrically into a smaller G1-phase cell and a larger S-phase cell and use conserved transcriptional regulators arranged in modules to coordinate transcription with cell cycle progression [13-16] (Fig 1A). In *C. crescentus*, MucR1 and MucR2 were recently shown to negatively regulate numerous promoters that are activated by the cell cycle transcriptional regulator A (CtrA) in G1-phase. MucR orthologs control virulence functions in α-proteobacterial pathogens and symbionts, but can also control cell cycle-regulated promoters in *C. crescentus* [17-20]. MucR1/2 target promoters by way of an ancestral zinc finger-like fold and both proteins are present throughout the *C. crescentus* cell cycle [17, 21, 22] (Fig 1A). By contrast, the OmpR-like DNA-binding response regulator CtrA is activated by phosphorylation and is only present in G1 and late S-phase cells [23, 24], but not in early S-phase cells (Fig 1A). The promoter controlling

4

93   expression of the conserved DNA methyltransferase CcrM is among the targets activated by

94   phosphorylated CtrA (CtrA~P) in late S-phase [15, 17, 25-27]. CcrM introduces m6A marks at sites

95   harbouring the recognition sequence 5'-GANTC-3' (henceforth GANTCs) once passage of the DNA

96   replication fork leaves GANTCs hemi-methylated (Fig 1B). CcrM is an unstable protein degraded by

97   the ATP-dependent protease Lon throughout the cell cycle [28, 29]. Since the *ccrM* gene is expressed

98   only in late S-phase cells, the time of expression dictates when the unstable CcrM protein is present

99   during the cell cycle. CcrM no longer cycles when it is expressed from a constitutive promoter in

100   otherwise *WT* cells or when Lon is inactivated [28, 30].

101   **Fig 1. Regulation of *C. crescentus* cell cycle and methylation of the chromosome.**

102   (A) Schematic of the *C. crescentus* cell cycle and the regulatory interactions that control G1-phase

103   promoters. Transcription from G1-phase promoters is activated by phosphorylated CtrA (CtrA~P, in

104   blue) and repressed by MucR1/2. CtrA~P accumulates in pre-divisional and swarmer (SW) cells, and

105   is eliminated by regulated proteolysis in the stalked (ST) cell upon compartmentalization and at the

106   swarmer to stalked cell differentiation. The red bar indicates that MucR1/2 proteins are present at all

107   stages of the cell cycle. (B) Schematic of the chromosome replication and adenine methylation (m6A)

108   during the *C. crescentus* cell cycle. Chromosome replication and methylation are shown for the same

109   cell cycle stages depicted in panel A. In non-replicative SW cells (T10) the chromosome is methylated

110   on both strands. Upon differentiation into ST cells (T40), chromosome replication start from the origin

111   (blue star) located at the old cell pole; progression of the replisomes (orange dots) generates hemi-

112   methylated chromosomes (black and green lines represent respectively the methylated and

113   unmethylated strand; T70 and T100). The cell cycle-regulated adenine methyltransferase CcrM is

114   synthesized only in late pre-divisional cells, where it methylates the newly synthesized chromosome

115   strands. CcrM is then specifically proteolyzed by the Lon protease. The purple numbers indicate the

116   position along the chromosome of the *P169* (1), *P1149* (2) and *P2901* (3) promoters. T10, T40, T70

117   and T100 indicate the time after synchronization at which the samples for anti-MucR1 ChIP-Exo were

118   taken (see text).

119

120   With the advent of SMRT (single-molecule real-time) sequencing it is now possible to obtain

121   m6A-methylome information of bacterial genomes at single base pair resolution [31, 32]. A recent cell

122   cycle methylome analysis of *C. crescentus* by SMRT-sequencing revealed the large majority of

123   GANTCs switch from hemi-methylated to a full methylated state (m6A-marked GANTCs on both

124   strands) at the onset of CcrM expression [12]. Interestingly, a few sites were consistently

125   hypomethylated, indicating that site-specific mechanisms control local hypomethylation patterns.

126   Local hypomethylation patterns may arise if specific DNA-binding proteins and/or restricted local

127   chromosome topology block access of CcrM to such GANTCs. Here, we combine restriction enzyme

128   cleavage-deep sequencing (REC-Seq) with SMRT sequencing to unearth hypomethylated GANTCs in

129   the genomes of wild type (*WT*) and mutant *C. crescentus* and *S. meliloti*. We show that the conserved

130   transcriptional regulator MucR induces local m6A-hypomethylation by preventing CcrM from

131   accessing GANTCs during S-phase, but only when CcrM cycles. Since repression of MucR target

132   promoters is normally overcome in G1-phase, our data suggest that MucR is unable to shield GANTCs

133   when CcrM is artificially present in G1 cells. Lastly, we discovered that phosphate starvation

134   promotes methylation of specific MucR-shielded GANTCs, revealing an environmental override of

135   the control system that normally instates local hypomethylation patterns during the cell cycle.

136

137 **Results**

138 **Identification and analysis of hypomethylated GANTCs by restriction enzyme cleavage**

139 **(REC-Seq).**

140   Detection of hypomethylated sites by SMRT-sequencing requires sufficient sequencing depth

141   and sophisticated bioinformatic analysis to differentiate unmethylated GANTCs from methylated

142   ones. Since unmethylated GANTCs can be conveniently enriched for in *C. crescentus* by restriction

143   enzyme cleavage using the *Hin*fI restriction enzyme (which only cleaves unmethylated GANTCs)

6

144 [33], we sought to apply *Hin*fI-based cleavage followed by Illumina-based deep-sequencing (REC-

145 Seq) to identify hypomethylated GANTCs, similar to a previous procedure used for analysis of

146 hypomethylated m6A sites in the unrelated γ-proteobacterium *Vibrio cholerae* [34]. We tested REC-

147 Seq on *Hin*fI-treated genomic DNA (gDNA) from *C. crescentus* and, following bioinformatic

148 filtering, obtained a list of unprotected GANTCs scaling with *Hin*fI cleavage efficiency ("score" in S1

149 Table). Since nearly all GANTCs suggested to be consistently unmethylated by SMRT sequencing

150 [12] are represented as high scoring GANTCs in the REC-Seq (note the medium differences or limited

151 SMRT sequencing depth may explain the differences), we concluded that REC-Seq captures

152 hypomethylated GANTCs in scaling manner (see below where selected sites cleaved in *WT* are no

153 longer cleaved in the Δ*mucR1/2* mutant). Since CcrM also methylates GANTCs in other α-

154 proteobacteria [35, 36], we also determined the hypomethylated GANTCs on the multipartite genome

155 of *S. meliloti* [37] by *Hin*fI REC-Seq and found such hypomethylated sites on the chromosome and

156 both megaplasmids (S1 Table).

157 To validate the *Hin*fI REC-Seq approach, we conducted REC-Seq (using the methylation-

158 sensitive *Mbo*I restriction enzyme) on gDNA from *Escherichia coli* K12 and *V. cholerae*, as

159 previously determined either by SMRT sequencing or REC-Seq [10, 34]. The Dam methylase

160 introduces m6A marks at GATCs in many γ-proteobacterial genomes [4] that protect from cleavage by

161 *Mbo*I. As known unmethylated sites in these control experiments indeed emerged with high score (S2

162 Table), we conclude that *Hin*fI REC-Seq is an efficient method to detect and quantitate GANTCs that

163 escape methylation by CcrM.

164

Several hypomethylated GANTCs in *C. crescentus* are MucR target sites.

166 Having identified hypomethylated GANTCs in the *C. crescentus* genome by *Hin*fI REC-Seq,

167 we noted that many high scoring GANTCs lie in regions that are occupied by MucR1/2 as determined

168 by previous chromatin-immunoprecipitation deep-sequencing (ChIP-Seq) analysis [17]. Of the hits

169 with a score higher than 100, one third lie in MucR1/2 target sequences, and the proportion is even

7

170   higher (50%) in the case of the 50 top hits (Table 1 and S1 Table). To test if MucR1/2 occludes these

171   GANTCs from methylation by CcrM, we conducted *Hin*fI-cleavage analysis of gDNA from *WT*

172   (NA1000) and Δ*mucR1/2* double mutant by qPCR (henceforth *Hin*fI-qPCR assay) at six MucR1/2

173   target sites. The *CCNA_00169* promoter (henceforth P*169*) contains four GANTCs; the *CCNA_02901*

174   promoter (P*2901*), the *CCNA_01149* promoter (P*1149*) and the *CCNA_01083* internal sequence

175   contain two GANTCs each; the *CCNA_02830* and *CCNA_03248* promoters (P*2830* and P*3248*) carry

176   one GANTC each (Fig 2A). A high percentage (100%) of methylation in the *Hin*fI-qPCR assay

177   indicates that *Hin*fI cannot cleave this site because of prior methylation by CcrM, whereas a low

178   percentage reflects efficient cleavage of the non-methylated DNA by *Hin*fI. In *WT* gDNA these six

179   MucR1/2-target sequences are almost completely cleaved by *Hin*fI, indicating that the GANTCs are

180   hypomethylated in the presence of MucR1/2. However, these sites are methylated and therefore not

181   cleaved by *Hin*fI in Δ*mucR1/2* cells (Fig 2B). As control for the specificity of the *Hin*fI-qPCR assay

182   we conducted the same analysis on sequences that are not MucR1/2 targets harbouring either i) a

183   hypomethylated GANTC (P$_{nagA}$), ii) several methylated GANTCs (P$_{podJ}$) or iii) a control sequence that

184   does not contain GANTCs (P$_{xylX}$). These controls revealed a level of amplification in the *Hin*fI-qPCR

185   assay as predicted (S1A Fig) and showed no difference between *WT* and Δ*mucR1/2* cells. Thus, only

186   hypomethylated sequences that are bound by MucR1/2 *in vivo* are converted to methylated GANTCs

187   in the absence of MucR1/2.

188   **Fig 2. MucR occludes specific GANTC sites from methylation.**

189   (A) Schematic of the loci carrying hypomethylated GANTCs occluded by MucR. The position of the

190   hypomethylated GANTCs identified by Kozdon et al. [12] is indicated by purple asterisks. Red lines

191   represent the occupancy of MucR1 and the values (x10^4 *per-base* coverage) calculated by the super-

192   resolution bioinformatic approach represent the average of the four time points (T10, T40, T70 and

193   T100, as described in the Methods). The MucR-dependent transcription start sites, determined by TSS-

194   EMOTE, are indicated by black (sense) and green (antisense) arrows. Dashed arrows indicate

195   transcription start sites found in both *WT* and Δ*mucR1/2* strains (*CCNA_01083-CCNA_01084*) or

196   down-regulated in the Δ*mucR1/2* strain compared to the *WT* (promoter of *CCNA_02831*). (B)

8

197   Methylation percentage of the loci shown in panel A in the *WT* and Δ*mucR1/2* strains, as determined

198   by *Hin*fI-qPCR.

199

200   SMRT sequencing of *WT* and Δ*mucR1/2* gDNA supported the result that these GANTCs carry

201   m6A marks as inferred by a high characteristic interpulse-duration (IPD) ratio observed in Δ*mucR1/2*

202   versus *WT* cells (S3 Table). Interestingly, this analysis also revealed eleven GANTCs with the inverse

203   behaviour, i.e. a low IPD ratio in Δ*mucR1/2* versus *WT* cells, suggesting that they no longer carry m6A

204   marks in the absence of MucR1/2. To confirm this result we conducted *Hin*fI-qPCR assays at two of

205   these GANTCs: the *CCNA_01248* promoter (P*1248*) and the *CCNA_03426* promoter (P*3426*). As

206   predicted by the methylome analysis, we observed that the methylation percentage of these GANTCs

207   was reduced in Δ*mucR1/2* versus *WT* (S1B Fig). On the basis of these experiments, we conclude that

208   MucR1/2 prevents m6A-methylation by CcrM at several MucR1/2-target sequences, but can also

209   facilitate methylation at other sites. This would likely occur by an indirect mechanism involving other

210   MucR-dependent DNA-binding proteins that compete with CcrM at certain GANTCs.

211   To obtain a global picture of hypomethylated GANTCs in the absence of MucR1/2, we

212   conducted REC-Seq analysis on gDNA extracted from the Δ*mucR1/2* strain (Table 1 and S1 Table).

213   Comparison of the REC-Seq data for *WT* and Δ*mucR1/2* cells (S2 Fig) supported the conclusion that

214   binding of MucR1/2 prevents methylation by CcrM, as the GANTCs tested by *Hin*fI-qPCR (shown in

215   Fig 2) have a high REC-Seq score in *WT* and a low REC-Seq score (or they are not detected) in the

216   Δ*mucR1/2* strain. Moreover, most of the GANTCs that show a strong decrease in score between *WT*

217   and Δ*mucR1/2* cells are also lying in regions directly bound by MucR1/2 (Table 1 and S1 Table),

218   based on ChIP-Exo (S4 Table) and published ChIP-Seq data [17].

219   **Table 1**. **REC-Seq in *WT* and Δ*mucR1/2*.**

220   GANTC sites with the highest (top 50) REC-Seq score in *WT C. crescentus* are listed. The complete

221   list of REC-Seq data for both *WT* and Δ*mucR1/2* strains is reported in Supplementary Table S1.

Position of GANTC site		REC-Seq Score in		Possible association	[1]Persistently unmethylated	[2]MucR target
		WT	ΔR1R2			
180973	180975	17756	1802	CCNA_00169		R1, R2
3781337	3781339	15184	8230	CCNA_R0079		
3992382	3992384	10934	5474	CCNA_03826/CCNA_03827		
738031	738033	10236	4678	CCNA_00681/CCNA_00682	Y	
3415859	3415861	9733	91	CCNA_03248	Y	R1, R2
2321619	2321621	9628	5563	CCNA_02167	Y	
2509257	2509259	9166	4171	CCNA_02366/CCNA_02367	Y	
1014421	1014423	8697	4155	CCNA_R0125/CCNA_00938/ CCNA_00939	Y	
1253987	1253989	7236	0	CCNA_01149	Y	R1, R2
1188431	1188433	7162	0	CCNA_01083	Y	R1
3431586	3431588	6912	116	CCNA_03262/CCNA_03263		R1, R2
3882781	3882783	6740	1061	CCNA_R0090/CCNA_03717/ CCNA_03718		
479267	479269	6634	14	CCNA_00466		R1, R2
458563	458565	6417	3	CCNA_00451	Y	
461814	461816	6211	4061	CCNA_00454/CCNA_03920	Y	
2086467	2086469	5523	19	CCNA_01944/CCNA_R0152		R1, R2
435741	435743	5173	0	CCNA_00425	Y	R1, R2
2056538	2056540	4840	2243	CCNA_01912/CCNA_01913		
1544245	1544247	4824	0	CCNA_01426	Y	R1, R2
1645085	1645087	4804	1875	CCNA_R0040		
1375838	1375840	4795	2782	CCNA_01247/CCNA_01248		
626625	626627	4669	3281	CCNA_00594/CCNA_R0112		
181127	181129	4639	0	CCNA_0169	Y	R1, R2
2335870	2335872	4636	571	CCNA_03962		
3885153	3885155	4552	247	CCNA_03719/CCNA_03721		
2984830	2984832	3903	0	CCNA_03980/CCNA_02830	Y	R1, R2
1567545	1567547	3901	3	CCNA_01457		R1, R2
1187860	1187862	3825	16	CCNA_01083	Y	R1, R2
2396048	2396050	3680	1531	CCNA_02246/CCNA_02247		
3056349	3056351	3578	0	CCNA_02901	Y	R1, R2
1187837	1187839	3298	7	CCNA_01083	Y	R1, R2
738020	738022	3255	1557	CCNA_00681/CCNA_00682	Y	
3056446	3056448	3249	0	CCNA_02901	Y	R1, R2
1906979	1906981	3099	17	CCNA_01779/CCNA_01780		R1, R2
181231	181233	2934	3	CCNA_00169	Y	R1, R2
3359883	3359885	2887	1682	CCNA_03199		
1254029	1254031	2873	0	CCNA_01149	Y	R1, R2
713385	713387	2823	0	CCNA_00657	Y	R1, R2
181197	181199	2712	0	CCNA_00169	Y	R1, R2

3261049	3261051	2571	283	CCNA_03108		
3188019	3188021	2520	1834	CCNA_03032/CCNA_03033	Y	
3987164	3987166	2451	489	CCNA_R0199		
2889722	2889724	2404	0	CCNA_02726	Y	R1, R2
2591862	2591864	2365	124	CCNA_02452		
2044585	2044587	2309	1765	CCNA_01902		
3592546	3592548	2178	7814	CCNA_03426		
1690112	1690114	2126	1239	CCNA_01573/CCNA_01574		
902058	902060	2098	6	CCNA_00836		R1, R2
2426668	2426670	1824	108	CCNA_02275/CCNA_02277		
1544275	1544277	1765	0	CCNA_01426		R1, R2

(1) Sites labelled with Y were identified as persistently unmethylated during the cell cycle by Kozdon et al. [12]

(2) Indicates whether a given GANTC site overlaps with MucR1 (R1) or MucR2 (R2) peaks identified by ChIP-Exo and ChIP-Seq (S4 Table and [17])

Conditions that impair local GANTC hypomethylation by MucR1/2.

Since CcrM is restricted to late S-phase and MucR1/2-repression is overcome in G1-phase [17, 28], we tested if MucR1/2-bound GANTCs are still hypomethylated when CcrM no longer cycles. To this end we used two strains: the Δlon::Ω (henceforth lon) mutant, as the Lon protease is responsible for degradation of CcrM throughout the cell cycle and upon inactivation of Lon the CcrM protein accumulates also in G1-cells, although it is only synthesized in S-phase [28, 29], and a strain with a second copy of the $ccrM$ gene under control of the constitutive P_{lac} promoter (integrated at the $ccrM$ locus, $ccrM$::P_{lac}-$ccrM$) [30, 33]. Indeed, HinfI-qPCR analysis revealed that the fraction of methylated P169, P1149 and P2901 GANTCs increases in lon mutant and $ccrM$::P_{lac}-$ccrM$ strain relative to WT cells (Fig 3A).

To exclude that constitutive presence of CcrM simply prevents MucR binding to DNA because CcrM outnumbers and therefore outcompetes MucR, we conducted several control experiments to demonstrate the specificity of the methylation control at these GANTCs. First, immunoblotting experiments revealed that MucR1/2 levels were maintained in the lon and $ccrM$::P_{lac}-$ccrM$ strains compared to WT (Fig 3C). Second, overexpression of either WT MucR1 or of an N-terminally extended (dominant-negative) MucR1 variant from P_{van} on a high copy plasmid (pMT335)

11

242   [17, 38] did not prevent methylation of P*169*, P*1149* and P*2901* GANTCs in *lon* mutant cells (Fig 3A)

243   or alter CcrM steady-state levels (S1C Fig). Conversely, constitutive expression of CcrM from the

244   same vector (pMT335) in *WT* cells recapitulated the effect on methylation of the P*169*, P*1149* and

245   P*2901* GANTCs (Fig 3B). Similarly, methylases of *Thermoplasma acidophilum* (*TA*), *Helicobacter*

246   *pylori* (*HP*) or *Haemophilus influenzae* (*Hinf*), which also specifically methylate GANTCs but are not

247   related to α-proteobacterial CcrM, also lead to methylation of these hypomethylated GANTCs when

248   expressed from pMT335 (Fig 3B). By contrast, the methylation state of GANTCs at the *parS* locus

249   was not significantly altered by the expression of the methylases or by the *lon* mutation (S1D Fig). On

250   the basis that CcrM and unrelated methylases are able to compete against MucR1/2 for methylation of

251   P*169*, P*1149* and P*2901* GANTCs when expressed constitutively, we hypothesize that MucR1/2 no

252   longer efficiently compete with CcrM in G1-phase when both proteins are present at this time (Fig 3A,

253   3B).

254   **Fig 3. Hypomethylation by MucR is impaired in G1-phase cells.**

255   (A) Methylation percentage of the *P169*, *P1149* and *P2901* sequences in strains in which the

256   methyltransferase CcrM is stabilised. The *Hin*fI-qPCR analysis indicates that methylation is increased

257   in cells carrying P$_{lac}$-*ccrM* or the *lon* mutation. In the case of the *lon* mutant, the methylation of *P169*,

258   *P1149* and *P2901* is not affected by increased levels of MucR1 [*R1*: P$_{van}$-*mucR1*, *R1 long*: N-

259   terminally extended dominant-negative MucR1 variant expressed from P$_{van}$ on pMT335]. (B)

260   Methylation percentage of the *P169*, *P1149* and *P2901* sequences in *WT* cells that constitutively

261   express *ccrM* or heterologous GANTC-methylases from P$_{van}$ on pMT335 (TA, *Thermoplasma*

262   *acidophilum*; HP, *Helicobacter pylori*; hinf, *Haemophilus influenzae*). (C) Immunoblot showing the

263   steady-state levels of CcrM, MucR1 and MucR2 in *WT* cells as well as the P$_{lac}$-*ccrM*, *lon* and

264   Δ*mucR1/2* strains. Molecular size standards are indicated on the right as blue lines with the

265   corresponding values in kDa. (D) Genome-wide occupancy of MucR1 in synchronised *WT* cells at

266   four different time points as determined by ChIP-Exo and super-resolution bioinformatic analysis:

267   swarmer (T10), stalked (T40), early pre-divisional (T70) and late pre-divisional cells (T100). The *x*

268   axis represents the nucleotide position on the genome, whereas the *y* axis shows the enrichment ratio

12

269   (E.R.) for each promoter region as reported in the S4 Table (see Methods for a detailed description).

270   (E) Heat map of the enrichment ratios of selected loci (those that contain hypomethylated GANTCs

271   occluded by MucR, see Fig 2) at the four time points after synchronization. The *pilA* locus is shown as

272   comparison as it is a well-characterized target of MucR [17]. The heat map shows that MucR1 is

273   constitutively associated with these loci.

274

275   To test if MucR1 binds to its targets in G1-phase, we conducted chromatin-

276   immunoprecipitation-followed by deep-sequencing of exonuclease treated fragments (ChIP-Exo), a

277   technique with enhanced resolution compared to conventional ChIP-Seq [39]. We treated with the

278   anti-MucR1 antibody chromatin prepared from synchronized cells at four different time points after

279   synchronization [10 min (T10, G1 phase), 40 min (T40, G1-to-S transition), 70 min (T70, early S-

280   phase), 100 min (T100, late S-phase) (Fig 1B)] and used a bioinformatic algorithm to define the

281   binding sites at super-resolution (see Methods and [40]). Surprisingly, the binding profiles at the four

282   time points appeared to be nearly congruent (Fig 3D) and quantification of the enrichment ratio failed

283   to reveal major changes of MucR1 binding to its targets during the cell cycle (Fig 3E and S4 Table).

284   On the other hand, conformational changes or altered dynamics of binding (i.e. dissociation constants,

285   on- and off-rates) that are undetectable by our methods might allow transcription from the MucR-

286   bound promoters in G1-phase. Transient release of DNA by MucR1/2 or changes in chromatin

287   conformation could provide access to competing DNA binding proteins such as CcrM, RNA

288   polymerase (RNAP) and other transcription factors (like CtrA) in G1-phase to induce methylation or

289   firing of the MucR1/2 target promoters.

290

MucR-dependent hypomethylation regulates sense and anti-sense transcription.

292   As MucR1/2 regulates the methylation state of the aforementioned GANTCs, we wondered if

293   the MucR1/2-targets P*169*, P*1149* and P*2901* display promoter activity in a MucR1/2-dependent

294   and/or methylation-dependent manner. To this end, we conducted LacZ (β-galactosidase)-based

295   promoter probe assays of P*169*-, P*1149*- and P*2901-lacZ* transcriptional reporters (driving expression

296   of a promoterless *lacZ* gene) in *WT* and Δ*mucR1/2* cells and observed that LacZ activity of all

297   reporters was elevated in Δ*mucR1/2* cells versus *WT* (Fig 4A-C). The increase was less dramatic for

298   P*169-lacZ* (156 ± 5.8 % relative to *WT*) than for P*1149*- and P*2901-lacZ* (439 ± 7.4 and 385 ± 40 %,

299   respectively). We then asked if promoter activity is augmented when cycling of CcrM is prevented.

300   Indeed, the P*169*-, P*1149*- and P*2901-lacZ* reporters indicated an increase in promoter activity in the

301   *lon* mutant and P$_{lac}$-*ccrM* strains compared to *WT* (Fig 4D). Importantly, no increase in LacZ activity

302   was observed in *lon* and P$_{lac}$-*ccrM* strains with other promoters (P*hvyA* and P*pilA*, Fig 4D) that are

303   bound by MucR1/2 and whose activity is increased in Δ*mucR1/2* cells [17, 41] but contain no

304   hypomethylated GANTCs. We further corroborated these results by showing that constitutive

305   expression of *C. crescentus* CcrM or the *T. acidophilum* GANTC-methylase from P$_{van}$ on pMT335 led

306   to an increase in P*169*-, P*1149*- and P*2901-lacZ* promoter activity (Fig 4E). Consistent with the fact

307   that in Δ*mucR1/2* cells these promoters are no longer hypomethylated, constitutive expression of

308   CcrM from P$_{lac}$-*ccrM* in Δ*mucR1/2* cells had no significant effect on P*169*-, P*1149*- and P*2901-lacZ*

309   promoter activity (Fig 4E).

310   **Fig 4. MucR and methylation by CcrM regulate transcription from target promoters.**

311   Beta-galactosidase activity of P*169* (*WT* promoter) and P*169** (with all GANTCs mutated to

312   GTNTCs) (A), P*2901* (*WT* promoter) and P*2901** (with the two GANTCs mutated to GTNTCs) (B)

313   and P*1149* (C) in *WT* and Δ*mucR1/2* cells. Mutation of MucR1/2 increases expression from P*169*-,

314   P*2901*- and P*1149-lacZ* independently from the presence of GANTCs. Values are expressed as

315   percentages (activity of *WT* promoter in *WT* cells set at 100%). (D) Beta-galactosidase activity of

316   P*169*-, P*1149*-, P*2901-lacZ* promoter probe constructs and two MucR-dependent control promoter

317   reporters (P$_{hvyA}$-*lacZ* and P$_{pilA}$-*lacZ*) in *WT* and cells that constitutively express *ccrM* (ccrM::P$_{lac}$-*ccrM*

318   or Δ*lon*::Ω). Methylation of the target promoters by CcrM increases the LacZ activity. Values are

319   expressed as percentages (activity in *WT* cells set at 100%). (E) Beta-galactosidase activity of P*169*-,

320   P*1149*- and P*2901-lacZ* in *WT* cells that constitutively express *ccrM* or a heterologous GANTC-

321   methylase from *T. acidophilum* (TA) on plasmid under control of P$_{van}$. Values are expressed as

322   percentages (activity in *WT* carrying the empty vector set at 100%). (F) Beta-galactosidase activity of

323   P*169*-, P*1149*- and P*2901-lacZ* in *WT* and Δ*mucR1/2* cells that constitutively express *ccrM*

324   (ccrM::P$_{lac}$-*ccrM*). Values are expressed as percentages (activity in *WT* cells set at 100%).

325

326   To determine if changing the GANTC methylation state (by mutation to GTNTC) in P*169*-

327   and P*2901-lacZ* (5 sites mutated for P*169, P169*; 2 sites for P*2901, P2901*) also affects promoter

328   activity, we measured LacZ activity of the mutant promoters in *WT* and Δ*mucR1/2* cells and found that

329   they still exhibited MucR1/2-dependency, as the P*169**- and P*2901**-*lacZ* were still strongly de-

330   repressed in the absence of MucR1/2 (Fig 4A, 4B). We also observed an increase (136% ± 6%) in

331   activity of P*169**-*lacZ* relative to P*169-lacZ* in *WT*, while the activity of P*2901**-*lacZ* was decreased

332   compared to P*2901-lacZ*. The mutations may alter the target sequence for other regulator(s) in

333   addition to the methylation properties, thereby affecting transcription directly or indirectly in a

334   positive or negative fashion [42, 43]. For example, P*2901* is bound by the master cell cycle regulator

335   CtrA *in vivo* and the Δ*mucR1/2* mutation is known to affect CtrA expression [17], whereas the P*169*

336   promoter is affected by the phosphate starvation response (see below) [44, 45].

337   LacZ-based assays are a general and indirect measurement of promoter activity, but they do

338   not pinpoint the transcription start sites (TSSs), thus cannot reveal the physical proximity of the TSS

339   relative to the hypomethylated GANTCs. To correlate transcriptional regulation of MucR1/2 and

340   hypomethylated GANTCs, we took advantage of the recently developed RNA-Seq-based strategy for

341   exact mapping of transcriptome ends (EMOTE) [46] that can also be used to map the (unprocessed)

342   5'ends of nascent transcripts that harbour triphosphate 5'end (5'-ppp). To this end, total RNA is first

343   treated with XRN1 (to remove monophosphorylated 5'ends) and then 5'-ppp transcripts are treated

344   with *E. coli* RppH, which converts the 5'ends to a monophosphorylated form that can be ligated to a

345   bar-tagged RNA oligo using T4 RNA ligase [46] (S3 Fig). Comparative TSS-EMOTE analysis in total

346   RNA extracted from *WT* and Δ*mucR1/2* cells unearthed several TSSs that are activated when

347   MucR1/2 is absent (arrows in Fig 2A, S5 Table). Importantly, several of these TSSs were detected in

348 close proximity to the GANTCs within MucR1/2 target sequences, including P*2901*, P*2830*, P*3248*

349 and *CCNA_01083*. These results, therefore, validate the physical proximity and functional interplay

350 between MucR1/2 and hypomethylated GANTCs. While for weak MucR1/2 target promoters the

351 sequencing depth may have limited their detection by TSS-EMOTE, this analysis unexpectedly

352 revealed several MucR-dependent antisense transcripts with potential regulatory roles (green arrows in

353 Fig 2A). We validated the MucR1/2-dependency of two such antisense promoters (P*2902*_AS and

354 P*3247*_AS) by LacZ-promoter probe assays and detected a substantial increase in activity of

355 P*2902*_AS-*lacZ* and P*3247*_AS-*lacZ* in Δ*mucR1/2* versus *WT* cells (S1E Fig), indicating that these

356 promoters (and the GANTCs within) are clearly MucR1/2 regulated in *C. crescentus*.

357

Control of hypomethylation of MucR-target promoters in α-proteobacteria

359 Knowing that MucR is functionally interchangeable in α-proteobacteria [17, 18] and that

360 hypomethylated GANTCs are also detected in the *S. meliloti* multipartite genome by *Hin*fI REC-Seq

361 (see above and S1 Table), we tested whether *S. meliloti* MucR also occludes GANTCs from

362 methylation by CcrM in target promoters. We compared the methylation of *WT* and *mucR*::Tn *S.*

363 *meliloti* gDNA by *Hin*fI REC-Seq and SMRT-sequencing (S1 and S3 Table). Guided by these data

364 sets, we validated hypomethylation of GANTCs at or near the *SMa1635* (SM2011_RS04470) and

365 *SMa2245* (SM2011_RS06125) genes by *Hin*fI-restriction/qPCR analysis. We chose these GANTCs,

366 located on the symbiotic megaplasmid pSymA, to take advantage of the *S. meliloti* multipartite

367 genome and to explore if MucR-control of hypomethylation also applies to episomal elements such as

368 a symbiotic megaplasmid. *Hin*fI-restriction/qPCR analysis revealed that these GANTCs are largely

369 hypomethylated in *WT* compared to *mucR*::*Tn* cells (Fig 5A, 5B). To confirm that these GANTCs are

370 indeed direct targets of *S. meliloti* MucR, we conducted quantitative ChIP (qChIP) experiments (Fig

371 5D) with chromatin from *S. meliloti WT* and *mucR*::*Tn* cells precipitated using antibodies to *C.*

372 *crescentus* MucR2 that recognize *S. meliloti* MucR on immunoblots (S4A Fig). The qChIP

373 experiments revealed that *S. meliloti* MucR indeed binds at or near the hypomethylated *SMa1635* and

16

374   *SMa2245* GANTCs of *WT* cells (Fig 5D), but not at a control site (*SMc01552*). Moreover, since CcrM

375   is restricted to late S-phase also in *S. meliloti* [14], we tested whether constitutive expression of *ccrM^Cc*

376   in *S. meliloti WT* cells affected the methylation of GANTCs at *SMa1635* and *SMa2245*. Ectopic

377   expression of *ccrM^Cc* from P_{lac} on pSRK vector [47] significantly increased the methylation of

378   *SMa1635* and *SMa2245*, showing that *S. meliloti* MucR no longer occludes GANTCs in target

379   promoters when cycling of CcrM is impaired (Fig 5C). Consistent with *SMa1635* and *SMa2245* being

380   MucR targets, LacZ-based promoter probe experiments (using P*a1635-lacZ* and P*a2245-lacZ*)

381   revealed that they are de-repressed in *S. meliloti mucR::Tn* cells compared to *WT* (Fig 5E) and that *S.*

382   *meliloti* MucR represses P*a1635-lacZ* and P*a2245-lacZ* in *C. crescentus WT* or *ΔmucR1/2* cells (Fig

383   5F). Importantly, when cycling of CcrM in *C. crescentus* was prevented by P_{lac}-*ccrM* or the *lon*

384   mutation P*a1635-lacZ* and P*a2245-lacZ* activity was increased compared to the *WT* strain (Fig 5G).

385   Thus, MucR controls hypomethylation during α-proteobacterial cell cycle.

Fig 5. Hypomethylation control by MucR is conserved in α-proteobacteria.

387   (A) Schematic of the two MucR-dependent hypomethylated loci (*SMa1635* and *SMa2245*) identified

388   by SMRT-sequencing in the in *S. meliloti WT* genome. Position of the hypomethylated GANTCs is

389   indicated by purple asterisks. The blue arrows indicate the DNA fragments cloned for LacZ promoter

390   probe assays. (B) *Hin*fI-qPCR analysis showing that *SMa1635* and *SMa2245* are hypomethylated in *S.*

391   *meliloti WT* cells compared to *mucR::Tn* cells. (C) Constitutive expression of *ccrM^Cc* from P_{lac} on

392   pSRK [47] in *S. meliloti WT* cells increases the methylation percentage of *SMa1635* and *SMa2245*,

393   indicating that hypomethylation of GANTCs by MucR is also impaired in *S. meliloti* G1-phase cells.

394   (D) MucR occupancy at *SMa1635*, *SMa2245* and *SMc1552* (control) in *WT* and *mucR::Tn S. meliloti*

395   cells, as determined by qChIP using antibodies to *C. crescentus* MucR2. *SMa1635* and *SMa2245* are

396   bound by *S. meliloti* MucR, which suggests that hypomethylation of GANTCs at these loci is directly

397   due to occlusion by MucR. (E) Beta-galactosidase activity of P*a1635–lacZ* and P*a2245–lacZ* in *S.*

398   *meliloti* (fragments indicated by blue arrows in panel **A**). Both DNA fragments show a promoter

399   activity that is strongly de-repressed in *mucR::Tn* cells compared to the *WT* strain. Values are

400   expressed as percentages (activity in *WT* cells set at 100%). (F) Beta-galactosidase activity of P*a1635*

401   and P*a2245* in *C. crescentus WT* and Δ*mucR1/2* cells expressing *mucR^{Sm}*. Expression of *mucR^{Sm}* from

402   P*_{van}* on pMT335 decreases beta-galactosidase activity of P*a1635* and P*a2245*. Values are expressed as

403   percentages (activity in *WT* cells carrying the empty vector set at 100%). (G) Beta-galactosidase

404   activity of P*a1635* and P*a2245* in *C. crescentus WT, P_{lac}-ccrM* or *lon* cells. Values are expressed as

405   percentages (activity in *WT* cells set at 100%).

406

Environmental and systemic signals controlling hypomethylation patterns.

408   To determine if other systemic (cell cycle) signals can alter methylation patterns in α-

409   proteobacteria, we tested if CtrA can also occlude GANTC sites from methylation by CcrM. First, we

410   constructed a synthetic promoter in which three GANTCs overlapping two CtrA-boxes (one GANTC

411   in each CtrA box and one in between) were placed downstream of an attenuated *E. coli* phage T5

412   promoter on the *lacZ* promoter probe plasmid (Fig 6A). Next, we determined the methylation

413   percentage of the GANTCs in *WT C. crescentus* cells harbouring the resulting reporter plasmid by

414   *Hin*fI-qPCR analysis and found that the GANTCs are only partially methylated in *WT* cells, but

415   efficiently methylated when CcrM is expressed ectopically (Fig 6A). Thus, methylation patterns can

416   also emerge from competition between CcrM and other cell cycle regulators such as CtrA at

417   appropriately positioned GANTCs.

Fig 6. Cell cycle and environmental signals affect methylation patterns.

419   (A) Competition between CtrA and CcrM. Schematic of the synthetic promoter carrying an attenuated

420   *E. coli* phage T5 promoter followed by three GANTCs (purple asterisks) overlapping two CtrA-boxes

421   (in yellow). *Hin*fI-qPCR analysis shows that this sequence is hypomethylated in *WT* cells, whereas

422   constitutive expression of *ccrM* (P*_{lac}-ccrM*) increases the methylation percentage. This indicates that

423   DNA-binding proteins other than MucR can also occlude GANTCs from methylation. (B) Methylation

424   percentage of P*169* and P*1149* in phosphate-limiting conditions compared to rich medium (PYE),

425   determined by *Hin*fI-qPCR analysis. Phosphate starvation (6h) significantly increases the methylation

426   level of P*169* but not P*1149*. (C) Beta-galactosidase activity of P*169–lacZ* and *P169*–lacZ* (GANTCs

427   mutated to GTNTCs as in Fig 4A) in *WT* and Δ*mucR1/2* cells in rich medium and phosphate-limiting

428   conditions. Phosphate starvation induces transcription from P*169–lacZ* and *P169*–lacZ* independently

429   from the presence of MucR1/2. Values are expressed as percentages (activity in *WT* cells grown in

430   PYE set at 100%). (D) Beta-galactosidase activity of P*1149–lacZ* in *WT* and Δ*mucR1/2* cells in rich

431   medium and phosphate-limiting conditions. Phosphate starvation does not significantly affect the

432   activity of P*1149–lacZ*. Values are expressed as percentages (activity in *WT* cells grown in PYE set at

433   100%).

434

435   To explore if environmental signals can also affect local hypomethylation patterns, we took

436   advantage of the fact that expression of *CCNA_00169* (also known as *elpS*) is induced upon phosphate

437   starvation of *C. crescentus* cells [44, 45]. Accordingly, we compared the P*169* methylation patterns by

438   *Hin*fI-qPCR analysis of gDNA from *WT* cells grown in standard medium (PYE) and phosphate-

439   limiting conditions. This revealed a significant increase in P*169* GANTC methylation in phosphate-

440   limiting conditions compared to PYE (Fig 6B) and we observed a commensurate induction of P*169-*

441   *lacZ* and *P169*-lacZ* that was MucR1/2 independent (Fig 6C). Both the increase in P*169* GANTC

442   methylation and P*169-lacZ* activity are dependent on the phosphate-responsive transcriptional

443   regulator PhoB (S4B-C Fig), suggesting that PhoB can facilitate methylation of MucR-protected

444   GANTCs at P*169*. The result that no significant increase of the P*1149* methylation or P*1149-lacZ*

445   activity was seen when *WT* cells were grown in phosphate-limiting conditions compared to standard

446   PYE medium (or in Δ*phoB*::Ω cells compared to *WT*) argues against the possibility that changes in

447   CcrM expression or activity underlie the modified methylation pattern of P*169* (Fig 6B, 6D; S4B-C

448   Fig). Thus, P*169* provides an example of an environmental override for a promoter subject to local

449   hypomethylation control by the cell cycle transcriptional circuitry.

450

451   **Discussion**

452   The correlative changes between human genetic variability and local (hypo)methylation

453   prompt the question if and how such patterns are regulated by the cell cycle and/or environmental

454   cues. Taking advantage of bacterial genomes that are small enough for full-methylome analysis by

455   cutting-edge REC-Seq and SMRT-sequencing, we show that local m6A-hypomethylation exists in two

456   different α-proteobacterial lineages and that conserved cell cycle factors govern its establishment in

457   both systems. While in γ-proteobacterial lineages transcriptional regulators are also known to compete

458   with the Dam m6A methylase to occlude certain methylation sites, local hypomethylation patterning

459   has not been explored in the context of the transcriptional circuitry controlling progression of the (α-

460   proteo)bacterial cell cycle. In eukaryotes methylation heterogeneity involves 5-methyl-cytosines

461   introduced at CpG dinucleotides [2], but recently m6A marks, instated by unknown mechanisms, have

462   also been reported [6-8]. Reliable detection of methylation sites by SMRT-sequencing requires

463   extensive (25-fold) coverage for adenine methylation and even higher coverage for cytosine

464   methylation (250-fold coverage needed in some instances)[5]. Non-methylated sites are only reliably

465   detected by elimination of sites on which methylation is detected, thus leaving an element of

466   uncertainty for those sites classified as non-methylated based on the absence of the kinetic signature

467   for methylation. By contrast, REC-Seq with a methylation sensitive restriction enzyme was used here

468   to enrich for non-methylated sites in α-proteobacteria by *Hin*fI cleavage. The continuum of scores we

469   detected in these experiments points towards the use of REC-Seq in detecting loci whose methylation

470   is variable within a culture, for example phase variable loci [48, 49]. *Hin*fI REC-Seq revealed the

471   occurrence of non-methylated GANTCs in at least two α-proteobacterial genomes. Subsequent genetic

472   analyses showed that the determinants controlling hypomethylation are conserved in these bacteria,

473   but they are not encoded in eukaryotic genomes. However, at least one component, MucR, possesses

474   an ancestral zinc-finger-type DNA binding domain [22], a protein domain which is also wide-spread

475   in developmental regulation of eukaryotes [50]. The fact that MucR regulates expression of virulence

476   and cell cycle genes [17-20], has recently been shown to confine genetic exchange by generalized

477   transduction to G1-phase in *C. crescentus* via transcriptional regulation [41] and is responsible for

478   hypomethylation of specific loci on the chromosome or megaplasmids thus raises the possibility that

479   zinc-finger proteins may control (epigenetic) DNA transactions including local hypomethylation

480 during the eukaryotic cell cycle as well. In bacteria local methylation changes may correlate with

481 altered virulence behaviour and may underlie cell cycle-control in pathogens, endosymbionts or other

482 microbial systems. Methylation is known to influence virulence functions in γ-proteobacteria, often by

483 imposing bistability from phase-variable virulence promoters in subpopulations via transcriptional

484 regulators such as Lrp, Fur or OxyR [5, 9, 42, 48, 51-55]. Phenotypic heterogeneity in antibiotic drug

485 tolerance *in vivo* (a state known as persistence), which is acquired in a low fraction of bacterial cells,

486 may also underlie epigenetic changes induced stochastically by methylation, either deterministically

487 (during the cell cycle) or environmentally. Although no phase-variable promoters are currently known

488 for the α-proteobacteria, these bacteria offer the possibility to investigate the relationship of local

489 hypomethylation with cell cycle control, as both *C. crescentus* and *S. meliloti* are synchronizable and

490 exhibit comparable cell cycle control systems and transcription [13-15, 56]. However, as binding of

491 MucR to DNA is not impaired by methylation, the mechanisms underlying the increase in

492 transcription of target genes induced by methylation in α-proteobacteria (Fig 4D-F; Fig 5G) are likely

493 to be different from those described for γ-proteobacteria. Moreover, the α-proteobacteria lineage

494 includes the Rickettsiales order encompassing obligate intracellular pathogens, endosymbionts and the

495 extinct proto-mitochondrion from which the modern day mitochondria descended [57]. As MucR and

496 CcrM orthologs are not encoded in most Rickettsiales genomes, the determinants of hypomethylation

497 in this order must be different, if they do exist. Interestingly, endosymbionts from the genus

498 *Wolbachia* might provide a possible exception. Their genomes encode an unusual putative DNA

499 methylase in which a C-terminal pfam01555 methylase-domain is fused to a pfam02195 ParB-like

500 nuclease domain found in DNA-binding proteins and plasmid replication factors [58]. The sheltered

501 niche of obligate intracellular Rickettsia contrasts with that of free-living relatives that are exposed to

502 major environmental fluctuations.

503 In summary, our work shows that environmental regulatory responses like that to phosphate

504 limitation, which is particularly pertinent for bacteria living in aquatic ecosystems as *C. crescentus*,

505 are superimposed on (direct or indirect) hypo- or hyper-methylation control cued by the cell cycle. As

506 many hypomethylated sites occur upstream of genes encoding transcription factors (see S1 Table) and

21

507   transcription factors are often regulatory, it is conceivable that local hypomethylation is often induced

508   by *cis*-encoded site-specific DNA-binding proteins that can compete with DNA methylases for

509   overlapping target sites. The mechanism of DNA binding and temporal regulation of MucR remain to

510   be elucidated in detail in order to reveal why MucR shields certain target sites from methylation by

511   CcrM. Our work on MucR-dependent hypomethylation by *Hin*fI REC-Seq along with the

512   comprehensive analysis of hypomethylated sites in other α-proteobacterial genomes [10] indicates that

513   the functions controlled by hypomethylated promoters are distinct and generally not conserved among

514   different α-proteobacteria. This suggests that hypomethylation does not play a major role in the

515   regulation of the α-proteobacterial cell cycle, even though conserved cell cycle transcriptional

516   regulators govern hypomethylation patterns. If it is largely serendipitous which sites MucR shields

517   from methylation, it seems plausible that such hypomethylation control systems mediate species-

518   specific transcriptional adaptations in response to stresses via MucR, CcrM or other variables that

519   influence their binding, either directly or indirectly. For example, cell cycle controlled changes in local

520   chromosomal topologies mediated by DNA replication or nucleoid-associated factors [59, 60] could

521   exclude DNA methylases form specific target sites.

522

Materials and Methods

Strains and growth conditions

525   *Caulobacter crescentus* NA1000 [61] and derivatives were grown at 30°C in PYE (peptone-

526   yeast extract) or M2G (minimal glucose). For phosphate starvation, *Caulobacter* cells were grown in

527   1/5X PYE (5-fold diluted PYE except 1 mM $MgSO_4$ and 1 mM $CaCl_2$, supplemented with 0.2%

528   glucose). *Sinorhizobium meliloti* Rm2011 and derivatives were grown at 30°C in Luria broth (LB)

529   supplemented with $CaCl_2$ 2.5 mM and $MgSO_4$ 2.5 mM. *Escherichia coli* S17-1 *λpir* and EC100D were

530   grown at 37°C in LB. Swarmer cell isolation, electroporations, bi-parental matings and bacteriophage

531   φCr30-mediated generalized transductions were performed as previously described [62-65]. Nalidixic

532   acid, kanamycin, gentamicin and tetracycline were used at 20 (8 for *S. meliloti*), 20, 1 (10 for *E. coli*

533   and *S. meliloti*) and 1 (10 for *E. coli* and *S. meliloti*) μg/mL, respectively. Plasmids for β-galactosidase

534   assays were introduced into *S. meliloti* by bi-parental mating and into *C. crescentus* by electroporation.

535   Strains and plasmids constructions are detailed in the S1 Text file.

536

Extraction of genomic DNA and methylation by qPCR (*Hin*fI-restriction/qPCR)

538   Genomic DNA was extracted from mid-log phase cells (10 ml). Aliquots of DNA (0.5-1 μg)

539   were digested with *Hin*fI restriction endonuclease and used to determine the methylation percentage

540   by Real-Time PCR. Real-time PCR was performed using a Step-One Real-Time PCR system (Applied

541   Biosystems, Foster City, CA) using 0.05% of each DNA sample (5 μl of a dilution 1:100) digested

542   with *Hin*fI, 12.5 μl of SYBR green PCR master mix (Quanta Biosciences, Gaithersburg, MD) and

543   primers 10 μM each, in a total volume of 25 μl. A standard curve generated from the cycle threshold

544   (C_t) value of the serially diluted non-digested genomic DNA was used to calculate the methylation

545   percentage value for each sample. Average values are from triplicate measurements done per culture,

546   and the final data was generated from three independent cultures per strain and condition. The primers

547   used for Real-Time PCR are listed in Table B in the S1 Text file.

548

Genome-wide methylation analyses

550   SMRT (single-molecule real-time) sequencing libraries were prepared from gDNA extracted

551   from the four samples (*C. crescentus* and *S. meliloti WT* and *mucR* mutant strains) using the DNA

552   Template Prep Kit 2.0 (250bp - 3Kb, Pacific Biosciences p/n 001-540-726). Sequences generated by

553   the Pacific Bioscience RSII were aligned to the *C. crescentus* NA1000 or *S. meliloti* Rm2011 genomes

554   [37, 66, 67] using Blasr (https://github.com/PacificBiosciences/blasr) and the modification and

555   associated motifs patterns were identified applying the RS_Modification_and_Motif_Analyisis

556   protocol in SMRT Analysis (https://github.com/PacificBiosciences/SMRT-Analysis/wiki/SMRT-

557   Analysis-Software-Installation-v2.2.0). For each aligned base, a statistics measured as interpulse

558 duration (IPD) combined with a modification quality value (QV) would mark the methylation status.

559 On the one hand, a minimum QV of 45 is required for a position to be marked as methylated; on the

560 other hand, a maximum QV between 10 and 30 (depending on the observed kinetic detections

561 background in the sample), coupled with the requirement that such a score is observed on both strands,

562 would mean that a position, in an otherwise methylated motif, is unmethylated.

563   For REC-Seq (*r*estriction *e*nzyme *c*leavage–*seq*uencing) 1 µg of genomic DNA from *C.*

564 *crescentus* NA1000 and *S. meliloti* Rm2011 was cleaved with *Hin*fI, a blocked (5'biotinylated)

565 specific adaptor was ligated to the ends and the ligated fragments were then sheared to an average size

566 of 150-400 bp (Fasteris SA, Geneva, CH). Illumina adaptors were then ligated to the sheared ends

567 followed by deep-sequencing using a Hi-Seq Illumina sequencer, and the (50 bp single end) reads

568 were quality controlled with FastQC (http://www.bioinformatics.babraham.ac.uk/projects/fastqc/). To

569 remove contaminating sequences, the reads were split according to the *Hin*fI consensus motif (5'-

570 G^ANTC-3') considered as a barcode sequence using fastx_toolkit

571 (http://hannonlab.cshl.edu/fastx_toolkit/) (fastx_barcode_splitter.pl --bcfile barcodelist.txt --bol --

572 exact). Most of the reads (more than 90%) were rejected, and the reads kept were remapped to the

573 reference genomes [37, 66, 67] with bwa mem [68] and samtools [69] to generate a sorted bam file.

574 The bam file was further filtered to remove low mapping quality reads (keeping AS >= 45) and split

575 by orientation (alignmentFlag 0 or 16) with bamtools [70]. The reads were counted at 5' positions

576 using Bedtools [71] (bedtools genomecov -d -5). Both orientation count files were combined into a

577 bed file at each identified 5'-GANTC-3' motif (where reverse counts >=1 at position N+1 and forward

578 counts >=1 at position N-1) using a home-made PERL script. The *Hin*fI positions in the bed file were

579 associated with the closest gene using Bedtools closest [71] and the gff3 file of the reference genomes

580 [72]. The final bed file was converted to an MS Excel sheet (S1 and S2 Tables) with a homemade

581 script. For the *Mbo*I-based REC-Seq, the strategy was identical except that a different adaptor was

582 used for ligation after cleavage and the *Mbo*I consensus motif (5'-^GATC-3') was used as barcode for

583 filtering of *V. cholerae* O1 biovar El Tor [73] and *E. coli* K12 Ec100D gDNA mapped onto the

584 MG1655 genome [74].

24

585

ChIP-Exo on *C. crescentus* synchronized cells

587   *C. crescentus WT* cells for ChIP-Exo were taken at different time points after synchronization

588 (10, 40, 70 and 100 minutes). After cross-linking, chromatin was prepared as previously described

589 [17]. ChIP-Exo was performed with 2 μl of polyclonal antibodies to MucR1 at Peconic LCC

590 (http://www.peconicgenomics.com) (State College, PA), which provided standard genomic position

591 format files (BAM) as output using the SOLiD genome sequencer (Applied Biosystems). A custom

592 Perl script was then used to calculate the sequencing (read) coverage per base (*per-base* coverage) for

593 each ChIP-Exo sample. Next, we computed the enrichment ratio (ER) for each promoter region. To

594 this end, the Perl script extracted the *per-base* coverage of a 600 bp region for each ORF (from -500 to

595 +100 from the start codon for each ORF annotated in *C. crescentus* genome) and calculated the

596 average coverage for each of these regions. The resulting value was then normalized with respect to

597 the coverage of all the intergenic regions. This was done (by the Perl script) by selecting all the

598 intergenic regions in the *C. crescentus* genome, merging them and extracting the *per-base* coverage

599 for all these intergenic regions. The coverage was averaged for windows of 600 bp, shifting each

600 window by 100 bp, and the mean of all resulting values was computed. The ER for each promoter

601 region was therefore calculated as the ratio between the average coverage of the promoter region

602 divided by the mean obtained for the intergenic regions.

603

Transcriptional start sites mapping by exact mapping of transcriptome ends (EMOTE)

605   The transcription start sites in the NA1000 *WT* and the Δ*mucR1/2* mutant were determined by

606 TSS-EMOTE (Transcription Start Specific Exact Mapping Of Transcriptome Ends), a global assay

607 that reveals the sequence of the 20 first nucleotides of 5'-triphosphorylated RNA in a sample based on

608 an XRN-1 digest of transcripts lacking the 5' triphosphate ends [46]. The TSS-EMOTE protocol and

609 analyses were performed according to the scheme in S3 Fig and the detailed protocol described in

610 [75]. We used a Worst-Case (i.e.) smallest difference) model to compare the number of Unique

611 Molecular Identifiers between the two pairs of biological replicates (i.e. mutant vs. wild-type) and

612 provide additional information about relative expression for each of the detected TSSs. The full list of

613 detected TSSs is shown in S5 Table and TSSs at the relevant genomic loci are indicated by black

614 (sense) and green (antisense) arrows in Fig 2A.

615

β-galactosidase assays

617 β-galactosidase assays were performed at 30°C. Cells (50-200 µl) at OD_{660nm}=0.1-0.5 were

618 lysed with chloroform and mixed with Z buffer (60 mM Na_2HPO_4, 40 mM NaH_2PO_4, 10 mM KCl and

619 1 mM $MgSO_4$, pH 7) to a final volume of 800 µl. Two hundred µl of ONPG (o-nitrophenyl-β-D-

620 galactopyranoside, stock solution 4 mg/ml in 0.1 M potassium phosphate, pH 7) were added and the

621 reaction timed. When a medium-yellow colour developed, the reaction was stopped by adding 400 µl

622 of 1M Na_2CO_3. The OD_{420nm} of the supernatant was determined and the Miller units (U) were

623 calculated as follows: $U = (OD_{420nm}*1000)/(OD_{660nm}*time$ [in min] *volume of culture used [in ml]).

624 Error was computed as standard deviation (SD) of at least three independent experiments.

625

qChIP assay on *S. meliloti*

627 Samples for qChIP assay were prepared from mid-log phase *S. meliloti* cells as previously

628 described [17]. Two microliters of polyclonal antibodies to MucR2 were used for the

629 immunoprecipitation.

630 Real-time PCR was performed as described for *Hinf*I-restricted genomic DNA, using 0.5% of

631 each ChIP sample (5 µl of a dilution 1:10). A standard curve generated from the cycle threshold (C_t)

632 value of the serially diluted chromatin input was used to calculate the percentage input value for each

633 sample. Average values are from triplicate measurements done per culture, and the final data was

634 generated from three independent cultures per strain. The primers used for *SMa1635* and *SMa2245*

635 loci were the same as for the determination of the methylation percentage of these loci (Table B in S1

636 Text file).

637

Immunoblots

For immunoblots, protein samples were separated on SDS polyacrylamide gel, transferred to polyvinylidene difluoride (PVDF) Immobilon-P membranes (Merck Millipore) and blocked in PBS (phosphate saline buffer) 0.1% Tween20 and 5% dry milk. The anti-sera were used at the following dilutions: anti-CcrM (1:10'000) [26], anti-MucR1 [17] (1:10'000), anti-MucR2 [17] (1:10'000). Protein-primary antibody complexes were visualized using horseradish peroxidase-labelled anti-rabbit antibodies and ECL detection reagents (Merck Millipore).

Plasmids, primers, synthetic fragments and strains constructions are described in the S1 Text file.

Data Access

Deep-sequencing data are deposited in Gene Expression Omnibus database (GEO: GSE79880).

Acknowledgments

References

1.   Casadesus J, Low D. Epigenetic gene regulation in the bacterial world. Microbiol Mol Biol Rev. 2006;70(3):830-56. doi: 10.1128/MMBR.00016-06. PubMed PMID: 16959970.

2.   Schubeler D. Function and information content of DNA methylation. Nature. 2015;517(7534):321-6. doi: 10.1038/nature14192. PubMed PMID: 25592537.

3.   Arber W, Dussoix D. Host specificity of DNA produced by *Escherichia coli*. I. Host controlled modification of bacteriophage lambda. J Mol Biol. 1962;5:18-36. PubMed PMID: 13862047.

4.   Marinus MG, Casadesus J. Roles of DNA adenine methylation in host-pathogen interactions: mismatch repair, transcriptional regulation, and more. FEMS Microbiol Rev. 2009;33(3):488-503. doi: 10.1111/j.1574-6976.2008.00159.x. PubMed PMID: 19175412.

5.   Sanchez-Romero MA, Cota I, Casadesus J. DNA methylation in bacteria: from the methyl group to the methylome. Curr Opin Microbiol. 2015;25:9-16. doi: 10.1016/j.mib.2015.03.004. PubMed PMID: 25818841.

6.   Greer EL, Blanco MA, Gu L, Sendinc E, Liu J, Aristizabal-Corrales D, et al. DNA Methylation on N6-Adenine in *C. elegans*. Cell. 2015;161(4):868-78. doi: 10.1016/j.cell.2015.04.005. PubMed PMID: 25936839.

7.   Fu Y, Luo GZ, Chen K, Deng X, Yu M, Han D, et al. N6-methyldeoxyadenosine marks active transcription start sites in chlamydomonas. Cell. 2015;161(4):879-92. doi: 10.1016/j.cell.2015.04.010. PubMed PMID: 25936837.

8.   Zhang G, Huang H, Liu D, Cheng Y, Liu X, Zhang W, et al. N6-methyladenine DNA modification in Drosophila. Cell. 2015;161(4):893-906. doi: 10.1016/j.cell.2015.04.018. PubMed PMID: 25936838.

9.   Adhikari S, Curtis PD. DNA methyltransferases and epigenetic regulation in bacteria. FEMS Microbiol Rev. 2016;40(5):575-91. doi: 10.1093/femsre/fuw023. PubMed PMID: 27476077.

10.   Blow MJ, Clark TA, Daum CG, Deutschbauer AM, Fomenkov A, Fries R, et al. The Epigenomic Landscape of Prokaryotes. PLoS Genet. 2016;12(2):e1005854. doi: 10.1371/journal.pgen.1005854. PubMed PMID: 26870957.

11.   Collier J. Epigenetic regulation of the bacterial cell cycle. Curr Opin Microbiol. 2009;12(6):722-9. doi: 10.1016/j.mib.2009.08.005. PubMed PMID: 19783470.

12.   Kozdon JB, Melfi MD, Luong K, Clark TA, Boitano M, Wang S, et al. Global methylation state at base-pair resolution of the *Caulobacter* genome throughout the cell cycle. Proc Natl Acad Sci U S A. 2013;110(48):E4658-67. doi: 10.1073/pnas.1319315110. PubMed PMID: 24218615.

13.   Panis G, Murray SR, Viollier PH. Versatility of global transcriptional regulators in alpha-Proteobacteria: from essential cell cycle control to ancillary functions. FEMS Microbiol Rev. 2015;39(1):120-33. doi: 10.1093/femsre/fuu002. PubMed PMID: 25793963.

14.   De Nisco NJ, Abo RP, Wu CM, Penterman J, Walker GC. Global analysis of cell cycle gene expression of the legume symbiont *Sinorhizobium meliloti*. Proc Natl Acad Sci U S A. 2014;111(9):3217-24. doi: 10.1073/pnas.1400421111. PubMed PMID: 24501121.

15.   Laub MT, McAdams HH, Feldblyum T, Fraser CM, Shapiro L. Global analysis of the genetic network controlling a bacterial cell cycle. Science. 2000;290(5499):2144-8. doi: 8994 [pii]. PubMed PMID: 11118148.

16.   Hallez R, Bellefontaine AF, Letesson JJ, De Bolle X. Morphological and functional asymmetry in alpha-proteobacteria. Trends Microbiol. 2004;12(8):361-5. doi: 10.1016/j.tim.2004.06.002. PubMed PMID: 15276611.

17.   Fumeaux C, Radhakrishnan SK, Ardissone S, Theraulaz L, Frandi A, Martins D, et al. Cell cycle transition from S-phase to G1 in *Caulobacter* is mediated by ancestral virulence regulators. Nature communications. 2014;5:4081. doi: 10.1038/ncomms5081. PubMed PMID: 24939058.

18.   Mirabella A, Terwagne M, Zygmunt MS, Cloeckaert A, De Bolle X, Letesson JJ. *Brucella melitensis* MucR, an Orthologue of *Sinorhizobium meliloti* MucR, Is Involved in Resistance to Oxidative, Detergent, and Saline Stresses and Cell Envelope Modifications. J Bacteriol. 2013;195(3):453-65. doi: 10.1128/JB.01336-12. PubMed PMID: 23161025.

19.   Cooley MB, Kado CI. Mapping of the ros virulence regulatory gene of *A. tumefaciens*. Mol Gen Genet. 1991;230(1-2):24-7. PubMed PMID: 1660566.

20.   Mueller K, Gonzalez JE. Complex regulation of symbiotic functions is coordinated by MucR and quorum sensing in *Sinorhizobium meliloti*. J Bacteriol. 2011;193(2):485-96. doi: 10.1128/JB.01129-10. PubMed PMID: 21057009.

21.   Baglivo I, Russo L, Esposito S, Malgieri G, Renda M, Salluzzo A, et al. The structural role of the zinc ion can be dispensable in prokaryotic zinc-finger domains. Proc Natl Acad Sci U S A. 2009;106(17):6933-8. Epub 2009/04/17. doi: 10.1073/pnas.0810003106. PubMed PMID: 19369210.

22.   Malgieri G, Russo L, Esposito S, Baglivo I, Zaccaro L, Pedone EM, et al. The prokaryotic Cys2His2 zinc-finger adopts a novel fold as revealed by the NMR structure of *Agrobacterium tumefaciens* Ros DNA-binding domain. Proc Natl Acad Sci U S A. 2007;104(44):17341-6. doi: 10.1073/pnas.0706659104. PubMed PMID: 17956987.

23.   Domian IJ, Quon KC, Shapiro L. Cell type-specific phosphorylation and proteolysis of a transcriptional regulator controls the G1-to-S transition in a bacterial cell cycle. Cell. 1997;90(3):415-24.

24.   Quon KC, Marczynski GT, Shapiro L. Cell cycle control by an essential bacterial two-component signal transduction protein. Cell. 1996;84(1):83-93.

25.   Reisenauer A, Quon K, Shapiro L. The CtrA response regulator mediates temporal control of gene expression during the Caulobacter cell cycle. J Bacteriol. 1999;181(8):2430-9.

26.   Stephens C, Reisenauer A, Wright R, Shapiro L. A cell cycle-regulated bacterial DNA methyltransferase is essential for viability. Proc Natl Acad Sci USA. 1996;93(3):1210-4.

27.   Laub MT, Chen SL, Shapiro L, McAdams HH. Genes directly controlled by CtrA, a master regulator of the *Caulobacter* cell cycle. Proc Natl Acad Sci U S A. 2002;99(7):4632-7. Epub 2002/04/04. doi: 10.1073/pnas.062065699. PubMed PMID: 11930012.

28.   Wright R, Stephens C, Zweiger G, Shapiro L, Alley MR. *Caulobacter* Lon protease has a critical role in cell-cycle control of DNA methylation. Genes Dev. 1996;10(12):1532-42.

29.   Jonas K, Liu J, Chien P, Laub MT. Proteotoxic stress induces a cell-cycle arrest by stimulating Lon to degrade the replication initiator DnaA. Cell. 2013;154(3):623-36. doi: 10.1016/j.cell.2013.06.034. PubMed PMID: 23911325.

30.   Collier J, McAdams HH, Shapiro L. A DNA methylation ratchet governs progression through a bacterial cell cycle. Proc Natl Acad Sci U S A. 2007;104(43):17111-6. doi: 10.1073/pnas.0708112104. PubMed PMID: 17942674.

31.   Lluch-Senar M, Luong K, Llorens-Rico V, Delgado J, Fang G, Spittle K, et al. Comprehensive methylome characterization of *Mycoplasma genitalium* and *Mycoplasma pneumoniae* at single-base resolution. PLoS Genet. 2013;9(1):e1003191. doi: 10.1371/journal.pgen.1003191. PubMed PMID: 23300489.

32.   Fang G, Munera D, Friedman DI, Mandlik A, Chao MC, Banerjee O, et al. Genome-wide mapping of methylated adenine residues in pathogenic *Escherichia coli* using single-molecule real-time sequencing. Nat Biotechnol. 2012;30(12):1232-9. doi: 10.1038/nbt.2432. PubMed PMID: 23138224.

33.   Zweiger G, Marczynski G, Shapiro L. A *Caulobacter* DNA methyltransferase that functions only in the predivisional cell. J Mol Biol. 1994;235(2):472-85.

34.   Dalia AB, Lazinski DW, Camilli A. Characterization of undermethylated sites in *Vibrio cholerae*. J Bacteriol. 2013;195(10):2389-99. doi: 10.1128/JB.02112-12. PubMed PMID: 23504020.

35.   Kahng LS, Shapiro L. The CcrM DNA methyltransferase of *Agrobacterium tumefaciens* is essential, and its activity is cell cycle regulated. J Bacteriol. 2001;183(10):3065-75. Epub 2001/04/28. doi: 10.1128/JB.183.10.3065-3075.2001. PubMed PMID: 11325934.

36.   Robertson GT, Reisenauer A, Wright R, Jensen RB, Jensen A, Shapiro L, et al. The *Brucella abortus* CcrM DNA methyltransferase is essential for viability, and its overexpression attenuates intracellular replication in murine macrophages. J Bacteriol. 2000;182(12):3482-9.

37.   Capela D, Barloy-Hubler F, Gouzy J, Bothe G, Ampe F, Batut J, et al. Analysis of the chromosome sequence of the legume symbiont *Sinorhizobium meliloti* strain 1021. Proc Natl Acad Sci U S A. 2001;98(17):9877-82. doi: 10.1073/pnas.161294398. PubMed PMID: 11481430.

762   38.   Thanbichler M, Iniesta AA, Shapiro L. A comprehensive set of plasmids for vanillate- and
763   xylose-inducible gene expression in *Caulobacter crescentus*. Nucleic Acids Research.
764   2007;35(20):e137. doi: 10.1093/nar/gkm818.
765   39.   Mahony S, Pugh BF. Protein-DNA binding in high-resolution. Crit Rev Biochem Mol Biol.
766   2015;50(4):269-83. doi: 10.3109/10409238.2015.1051505. PubMed PMID: 26038153.
767   40.   Fioravanti A, Fumeaux C, Mohapatra SS, Bompard C, Brilli M, Frandi A, et al. DNA binding
768   of the cell cycle transcriptional regulator GcrA depends on N6-adenosine methylation in *Caulobacter*
769   *crescentus*   and   other   Alphaproteobacteria.   PLoS   Genet.   2013;9(5):e1003541.   doi:
770   10.1371/journal.pgen.1003541. PubMed PMID: 23737758.
771   41.   Ardissone S, Fumeaux C, Bergé M, Beaussart A, Theraulaz L, Radhakrishnan SK, et al. Cell
772   cycle   constraints   on   capsulation   and   bacteriophage   susceptibility.   eLife.   2014;3.   doi:
773   10.7554/eLife.03587. PubMed PMID: 25421297.
774   42.   Cota I, Bunk B, Sproer C, Overmann J, Konig C, Casadesus J. OxyR-dependent formation of
775   DNA methylation patterns in OpvABOFF and OpvABON cell lineages of *Salmonella enterica*.
776   Nucleic Acids Res. 2015. doi: 10.1093/nar/gkv1483. PubMed PMID: 26687718.
777   43.   Gonzalez D, Kozdon JB, McAdams HH, Shapiro L, Collier J. The functions of DNA
778   methylation by CcrM in *Caulobacter crescentus*: a global approach. Nucleic Acids Res. 2014. doi:
779   10.1093/nar/gkt1352. PubMed PMID: 24398711.
780   44.   Le Blastier S, Hamels A, Cabeen M, Schille L, Tilquin F, Dieu M, et al. Phosphate starvation
781   triggers production and secretion of an extracellular lipoprotein in *Caulobacter crescentus*. PLoS One.
782   2010;5(12):e14198. doi: 10.1371/journal.pone.0014198. PubMed PMID: 21152032.
783   45.   Lubin EA, Henry JT, Fiebig A, Crosson S, Laub MT. Identification of the PhoB Regulon and
784   Role of PhoU in the Phosphate Starvation Response of *Caulobacter crescentus*. J Bacteriol.
785   2015;198(1):187-200. doi: 10.1128/JB.00658-15. PubMed PMID: 26483520.
786   46.   Redder P. Using EMOTE to map the exact 5'-ends of processed RNA on a transcriptome-wide
787   scale. Methods Mol Biol. 2015;1259:69-85. doi: 10.1007/978-1-4939-2214-7_5. PubMed PMID:
788   25579580.
789   47.   Khan SR, Gaines J, Roop RM, 2nd, Farrand SK. Broad-host-range expression vectors with
790   tightly regulated promoters and their use to examine the influence of TraR and TraM expression on Ti
791   plasmid quorum sensing. Appl Environ Microbiol. 2008;74(16):5053-62. doi: 10.1128/AEM.01098-
792   08. PubMed PMID: 18606801.
793   48.   Cota I, Blanc-Potard AB, Casadesus J. STM2209-STM2208 (opvAB): a phase variation locus
794   of *Salmonella enterica* involved in control of O-antigen chain length. PLoS One. 2012;7(5):e36863.
795   doi: 10.1371/journal.pone.0036863. PubMed PMID: 22606300.
796   49.   Casadesus J, Low DA. Programmed heterogeneity: epigenetic mechanisms in bacteria. J Biol
797   Chem. 2013;288(20):13929-35. doi: 10.1074/jbc.R113.472274. PubMed PMID: 23592777.
798   50.   Klug A. The discovery of zinc fingers and their applications in gene regulation and genome
799   manipulation.   Annual   review   of   biochemistry.   2010;79:213-31.   doi: 10.1146/annurev-biochem-
800   010909-095056. PubMed PMID: 20192761.
801   51.   Cota I, Sanchez-Romero MA, Hernandez SB, Pucciarelli MG, Garcia-Del Portillo F,
802   Casadesus J. Epigenetic Control of *Salmonella enterica* O-Antigen Chain Length: A Tradeoff between
803   Virulence   and   Bacteriophage   Resistance.   PLoS   Genet.   2015;11(11):e1005667.   doi:
804   10.1371/journal.pgen.1005667. PubMed PMID: 26583926.
805   52.   Arnoldini M, Vizcarra IA, Pena-Miller R, Stocker N, Diard M, Vogel V, et al. Bistable
806   expression of virulence genes in salmonella leads to the formation of an antibiotic-tolerant
807   subpopulation. PLoS Biol. 2014;12(8):e1001928. doi: 10.1371/journal.pbio.1001928. PubMed PMID:
808   25136970.
809   53.   Broadbent SE, Davies MR, van der Woude MW. Phase variation controls expression of
810   *Salmonella* lipopolysaccharide modification genes by a DNA methylation-dependent mechanism. Mol
811   Microbiol. 2010;77(2):337-53. doi: 10.1111/j.1365-2958.2010.07203.x. PubMed PMID: 20487280.
812   54.   Peterson SN, Reich NO. Competitive Lrp and Dam assembly at the pap regulatory region:
813   implications for mechanisms of epigenetic regulation. J Mol Biol. 2008;383(1):92-105. doi:
814   10.1016/j.jmb.2008.07.086. PubMed PMID: 18706913.
815   55.   Atack JM, Srikhanta YN, Fox KL, Jurcisek JA, Brockman KL, Clark TA, et al. A biphasic
816   epigenetic   switch   controls   immunoevasion,   virulence   and   niche   adaptation   in   non-typeable

Haemophilus influenzae. Nature communications. 2015;6:7828. doi: 10.1038/ncomms8828. PubMed PMID: 26215614.

56.   Pini F, De Nisco NJ, Ferri L, Penterman J, Fioravanti A, Brilli M, et al. Cell Cycle Control by the Master Regulator CtrA in *Sinorhizobium meliloti*. PLoS Genet. 2015;11(5):e1005232. doi: 10.1371/journal.pgen.1005232. PubMed PMID: 25978424.

57.   Andersson SG, Zomorodipour A, Andersson JO, Sicheritz-Ponten T, Alsmark UC, Podowski RM, et al. The genome sequence of *Rickettsia prowazekii* and the origin of mitochondria. Nature. 1998;396(6707):133-40. doi: 10.1038/24094. PubMed PMID: 9823893.

58.   Ellegaard KM, Klasson L, Naslund K, Bourtzis K, Andersson SG. Comparative genomics of Wolbachia and the bacterial species concept. PLoS Genet. 2013;9(4):e1003381. doi: 10.1371/journal.pgen.1003381. PubMed PMID: 23593012.

59.   Rimsky S, Travers A. Pervasive regulation of nucleoid structure and function by nucleoid-associated proteins. Curr Opin Microbiol. 2011;14(2):136-41. doi: 10.1016/j.mib.2011.01.003. PubMed PMID: 21288763.

60.   Sobetzko P, Travers A, Muskhelishvili G. Gene order and chromosome dynamics coordinate spatiotemporal gene expression during the bacterial growth cycle. Proceedings of the National Academy of Sciences. 2012;109(2):E42–E50. doi: 10.1073/pnas.1108229109.

61.   Evinger M, Agabian N. Envelope-associated nucleoid from *Caulobacter crescentus* stalked and swarmer cells. J Bacteriol. 1977;132(1):294-301.

62.   Ely B. Genetics of *Caulobacter crescentus*. Methods Enzymol. 1991;204:372-84.

63.   Chen JC, Viollier PH, Shapiro L. A membrane metalloprotease participates in the sequential degradation of a *Caulobacter* polarity determinant. Mol Microbiol. 2005;55(4):1085-103. Epub 2005/02/03. doi: 10.1111/j.1365-2958.2004.04443.x. PubMed PMID: 15686556.

64.   Viollier PH, Shapiro L. A lytic transglycosylase homologue, PleA, is required for the assembly of pili and the flagellum at the *Caulobacter crescentus* cell pole. Mol Microbiol. 2003;49(2):331-45. Epub 2003/06/28. doi: 3576 [pii]. PubMed PMID: 12828633.

65.   Viollier PH, Thanbichler M, McGrath PT, West L, Meewan M, McAdams HH, et al. Rapid and sequential movement of individual chromosomal loci to specific subcellular locations during bacterial DNA replication. Proc Natl Acad Sci U S A. 2004;101(25):9257-62. doi: 10.1073/pnas.0402606101. PubMed PMID: 15178755.

66.   Marks ME, Castro-Rojas CM, Teiling C, Du L, Kapatral V, Walunas TL, et al. The genetic basis of laboratory adaptation in *Caulobacter crescentus*. J Bacteriol. 2010;192(14):3678-88. doi: 10.1128/JB.00255-10. PubMed PMID: 20472802.

67.   Nierman WC, Feldblyum TV, Laub MT, Paulsen IT, Nelson KE, Eisen J, et al. Complete genome sequence of *Caulobacter crescentus*. Proc Natl Acad Sci U S A. 2001;98(7):4136-41.

68.   Li H, Durbin R. Fast and accurate long-read alignment with Burrows-Wheeler transform. Bioinformatics. 2010;26(5):589-95. doi: 10.1093/bioinformatics/btp698. PubMed PMID: 20080505; PubMed Central PMCID.

69.   Li H. A statistical framework for SNP calling, mutation discovery, association mapping and population genetical parameter estimation from sequencing data. Bioinformatics. 2011;27(21):2987-93. doi: 10.1093/bioinformatics/btr509. PubMed PMID: 21903627.

70.   Barnett DW, Garrison EK, Quinlan AR, Stromberg MP, Marth GT. BamTools: a C++ API and toolkit for analyzing and managing BAM files. Bioinformatics. 2011;27(12):1691-2. doi: 10.1093/bioinformatics/btr174. PubMed PMID: 21493652.

71.   Quinlan AR, Hall IM. BEDTools: a flexible suite of utilities for comparing genomic features. Bioinformatics. 2010;26(6):841-2. doi: 10.1093/bioinformatics/btq033. PubMed PMID: 20110278.

72.   Kersey PJ, Allen JE, Armean I, Boddu S, Bolt BJ, Carvalho-Silva D, et al. Ensembl Genomes 2016: more genomes, more complexity. Nucleic Acids Res. 2016;44(D1):D574-80. doi: 10.1093/nar/gkv1209. PubMed PMID: 26578574.

73.   Heidelberg JF, Eisen JA, Nelson WC, Clayton RA, Gwinn ML, Dodson RJ, et al. DNA sequence of both chromosomes of the cholera pathogen *Vibrio cholerae*. Nature. 2000;406(6795):477-83.

74.   Riley M, Abe T, Arnaud MB, Berlyn MKB, Blattner FR, Chaudhuri RR, et al. *Escherichia coli* K-12: a cooperatively developed annotation snapshot—2005. Nucleic Acids Research. 2006;34(1):1-9. doi: 10.1093/nar/gkj405.

872   75.   Prados J., Linder P., Redder P. TSS-EMOTE, a refined protocol for a more complete and less
873   biased global mapping of trnscription start sites in bacterial pathogens. BMC genomics. 2016;17:849.
874   doi: 10.1186/s12864-016-3211-3.

875

876 **S1 Text file**

877 **Strains and plasmids construction.**

878 <u>Table A. Strains and plasmids used in this study.</u>

879 <u>Table B. Oligonucleotides used in this study.</u>

880

881 **S1 Fig. Controls for methylation percentage by *Hin*fI-qPCR and MucR-dependent**

882 **antisense transcription.**

883 (A) Methylation percentage of control loci in the *WT* and Δ*mucR1/2* strains, as determined by *Hin*fI-

884 qPCR: P_{nagA} (hypomethylated, MucR-independent), P_{xylX} (no GANTCs), P_{podJ} (fully methylated,

885 MucR-independent). The controls show that MucR does not affect the methylation of sequences that

886 are not its direct targets. (Note that as P_{xylX} contains no GANTCs, the label on the y-axis should not be

887 interpreted as methylation but cleavage percentage). (B) Methylation percentage of P*1248* and P*3426*

888 determined by *Hin*fI-qPCR analysis. The graphs show that these sequences are hypomethylated in the

889 Δ*mucR1/2* compared to the *WT* strain, as predicted by the SMRT-sequencing and REC-Seq. This

890 suggests that other DNA-binding proteins, directly or indirectly MucR-dependent, can also occlude

891 GANTCs from methylation. (C) Immunoblot anti-CcrM in *WT* and *lon* mutant cells carrying an empty

892 vector, P_{van}-*mucR1* or P_{van}-*mucR1* long (dominant negative form of MucR1 with an N-terminal

893 extension). Over-expression of MucR1 does not affect the steady state levels of CcrM (arrow). Note

894 that CcrM levels are elevated in the *lon* mutant strain as the protein is stabilized. Molecular size

895 standards are indicated on the right as blue lines with the corresponding values in kDa. (D)

896 Methylation percentage of the *parS* locus in *C. crescentus WT* cells carrying the empty vector, the

897 heterologous methylases (*TA*, *HP*, *hinf*) under control of P_{van} on pMT335, P_{lac}-*ccrM* and in the *lon*Ω

898 mutant. Stabilisation of CcrM or constitutive expression of heterologous methylases does not affect

899 the methylation state of GANTCs at the *parS* locus. (E) Beta-galactosidase activity of two MucR-

900   dependent antisense promoters identified by TSS-EMOTE. Values are expressed as percentages

901   (activity in *WT* cells set at 100%).

902

S2 Fig. Rec-Seq comparison of GANTC methylation in *WT* and Δ*mucR1/2*.

903

904   The Rec-Seq score of each GANTC site in *WT* and Δ*mucR1/2 C. crescentus* was normalized according

905   to the total number of reads obtained for the strains. The graph represents the difference between the

906   normalized score obtained for the *WT* and the normalized score for the Δ*mucR1/2* strain for each

907   GANTC site according to the position along the chromosome. Positive values (in blue) indicate

908   hypomethylation in the *WT*, whereas negative values (in red) indicate hypomethylation in the

909   Δ*mucR1/2* strain. The GANTCs verified by *Hin*fI-qPCR are indicated.

910

S3 Fig. Flowchart of the EMOTE assay.

911

912   RNA is shown as thin lines and DNA as thick lines, double lines represent Illumina adaptors. (A)

913   Cellular RNAs exist as primary transcripts with a triphosphorylated 5'end (PPP, red line) and

914   processed transcripts with either a monophosphorylated 5'end (P, dashed grey line) or a non-

915   phosphorylated 5'-OH end (straight grey line). The asterisk indicates the ends of interest. XRN1 is

916   used to remove 5' monophosphorylated RNA (grey dotted line) from the total RNA samples. (B)

917   Treatment with *E. coli* RppH converts the 5' triphosphorylated end of primary transcripts to a

918   monophosphorylated 5'end, a substrate for ligation (C, D) to the Rp6 synthetic oligonucleotide with

919   T4 RNA ligase 1, which does not accept triphosphorylated or non-phosphorylated substrates. A mock

920   reaction is performed at this stage in the absence of RppH to control for background (non-specific)

921   signals. (E, F) Reverse transcription generates cDNA from both non-phosphorylated and Rp6-ligated

922   RNA. Open arrows indicate polymerase extension. (G) Only cDNA from Rp6-ligated (and therefore

923   originally triphosphorylated) RNA is amplified by the primers that add EMOTE barcodes (xxx) and

924   Illumina adaptors. (H) Illumina sequencing (50 nucleotides) from the "A" end (see panel G) results in

925   reads that have the specific EMOTE barcode of the original RNA sample, the Rp6 sequence and the

926   first 20 nucleotides of the original triphosphorylated RNA, permitting exact identification of the

927   original 5' end.

928

929   **S4 Fig. Antibodies against *C. crescentus* MucR2 specifically recognize *S. meliloti* MucR.**

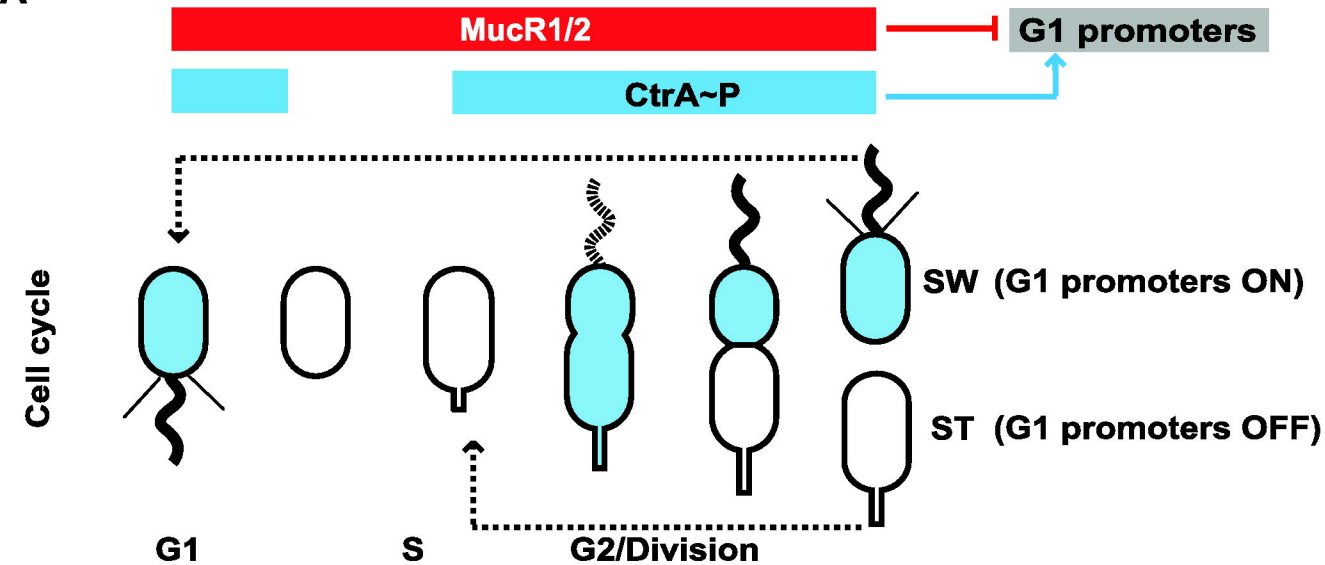930   **Methylation and induction of P*169* are PhoB-dependent.**

931   (A) Immunoblot on *C. crescentus* and *S. meliloti* total cell extracts showing that the polyclonal

932   antibodies against *C. crescentus* MucR2 specifically recognize *S. meliloti* MucR (SMc00058).

933   Molecular size standards are indicated on the right as blue lines with the corresponding values in kDa.

934   (B) Methylation percentage of P*169* and P*1149* in phosphate-limiting conditions compared to rich

935   medium (PYE) in *WT* and Δ*phoB*::Ω cells, determined by *Hinf*I-qPCR analysis. The graphs show that

936   the increase in the methylation state of P*169* is dependent on the presence of the conserved

937   transcriptional regulator PhoB. (C) Beta-galactosidase activity of P*169–lacZ* and P*1149–lacZ* in *WT*

938   and Δ*phoB*:: Ω cells in rich medium and phosphate-limiting conditions. The induction of P*169-lacZ* is

939   specifically dependent on the presence of PhoB. Values are expressed as percentages (activity in *WT*

940   cells grown in PYE set at 100%).

941

942   **S1 Table.** REC-Seq *Hin*fI analysis of *C. crescentus* and *S. meliloti* genomic DNA. In both cases, wild

943   type and *mucR* mutant strains were analysed. For the GANTC sites with a score higher than 100 in the

944   *WT C. crescentus*, REC-Seq data were compared to available ChIP-Seq [17] and SMRT-Sequencing

945   data [12]. The GANTCs tested by HinfI-qPCR assay are highlighted in yellow. The 50 GANTCs with

946   the highest score in *WT C. crescentus* are those shown also in Table 1.
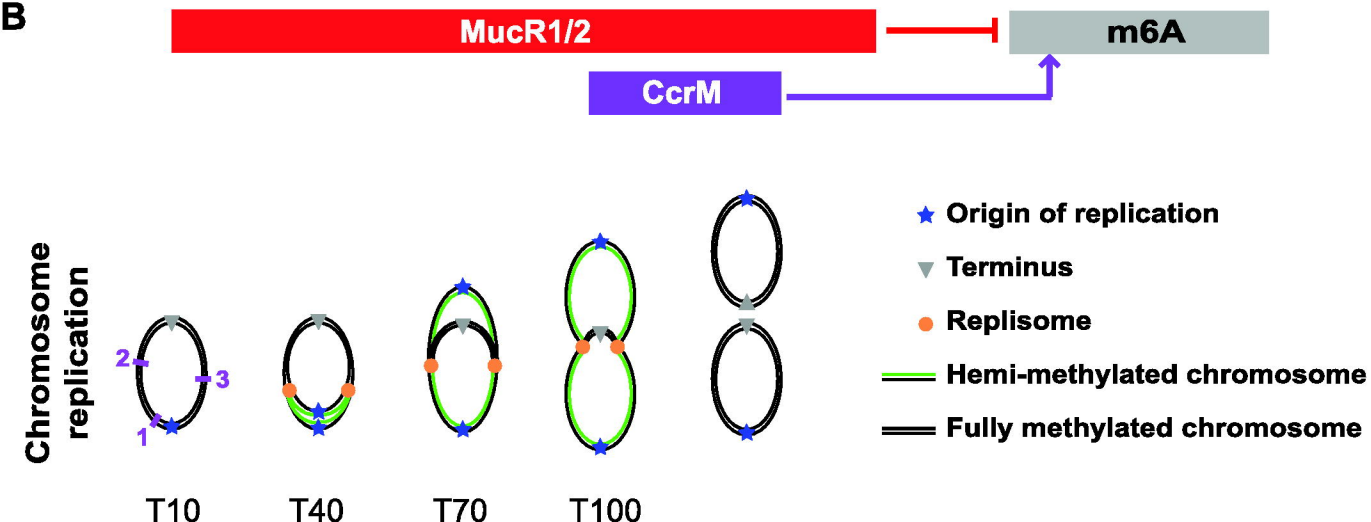
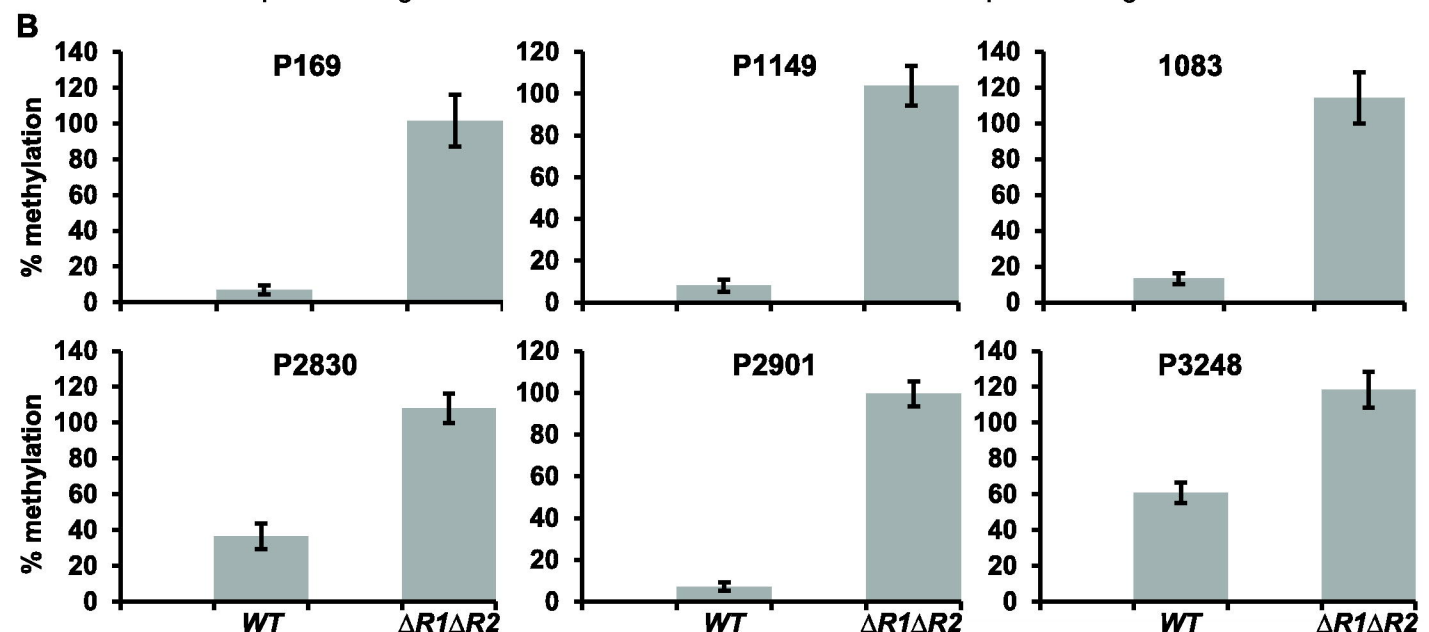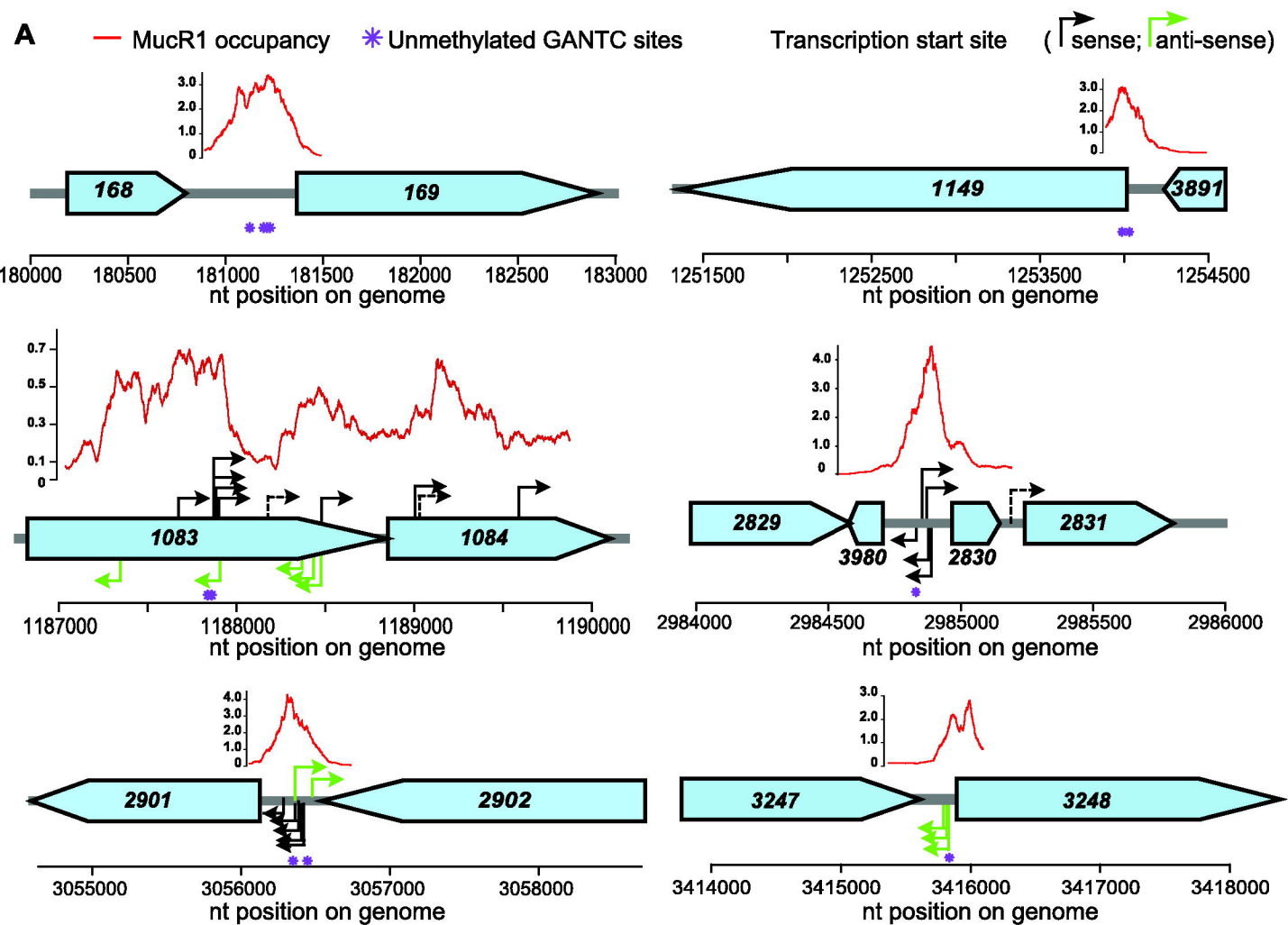947   **S2 Table.** REC-Seq *Mbo*I analysis of *E. coli K12* and *Vibrio cholerae* genomic DNA.

948 **S3 Table.** Non-methylated GANTCs predicted from SMRT analysis of *WT* and *mucR* mutant in *C.*

949 *crescentus* and *S. meliloti* genomic DNA.

950 **S4 Table.** ChIP-Exo analysis of MucR1 occupancy at different time points (T10, T40, T70, T100)

951 during the *C. crescentus* cell cycle.

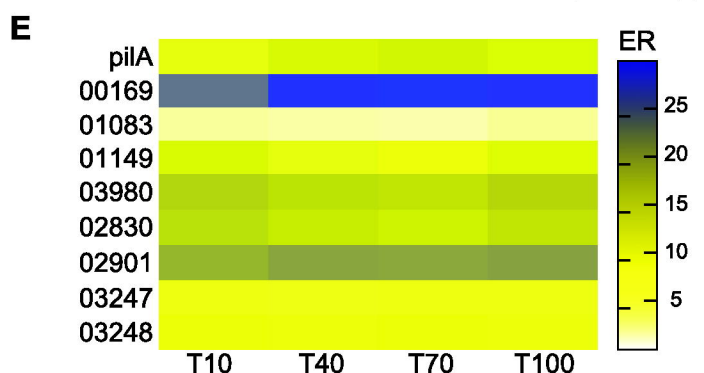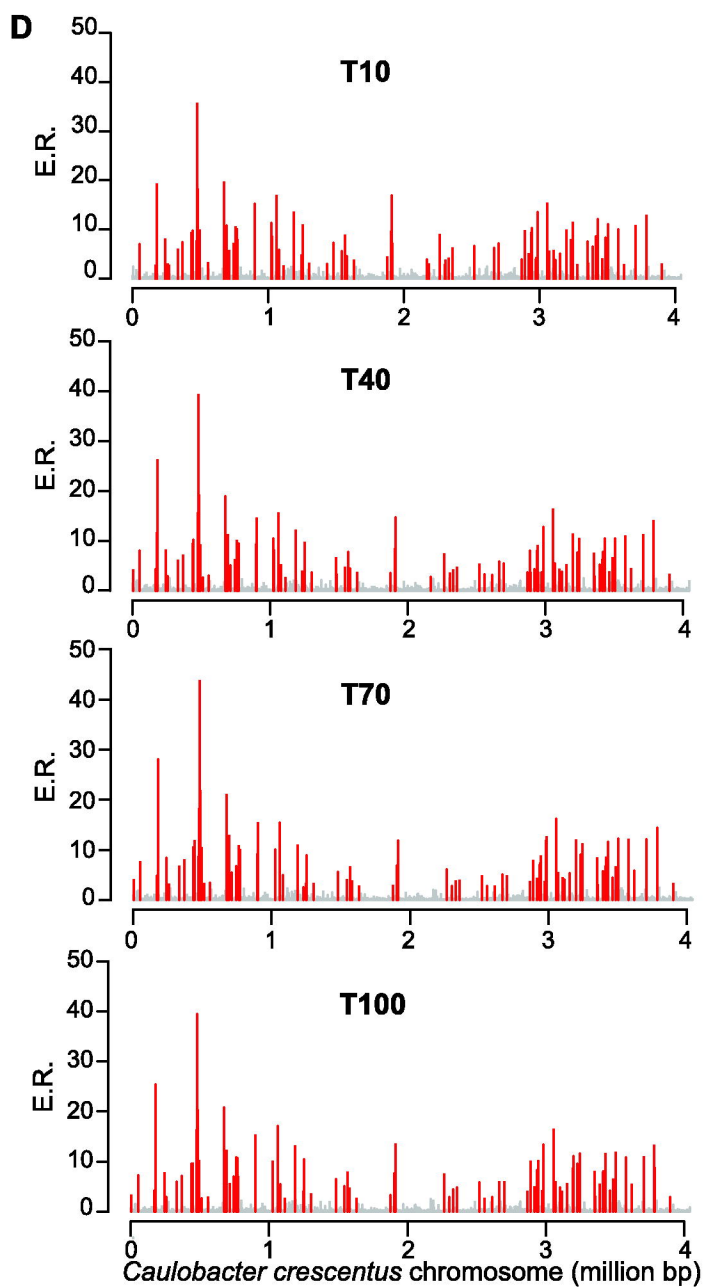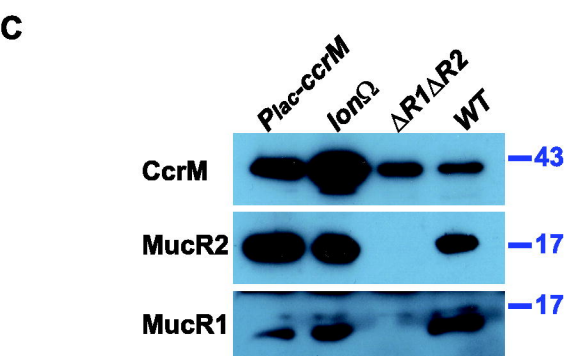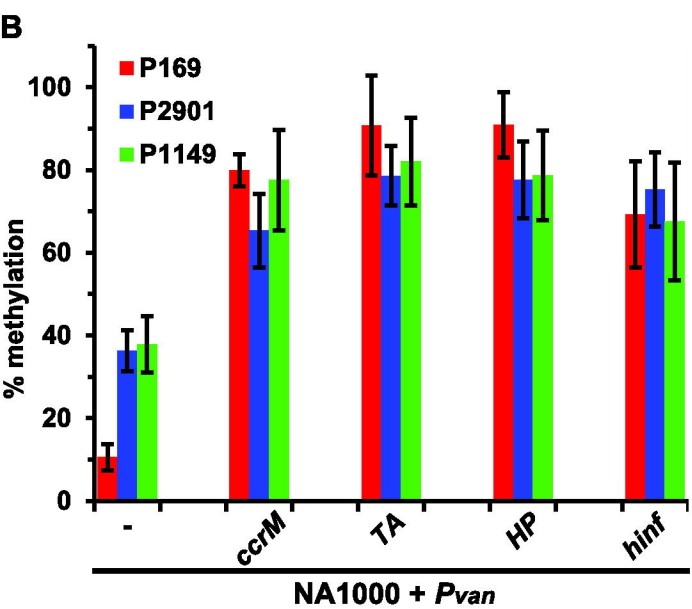952 **S5 Table.** TSS-EMOTE analysis of transcription start sites in *WT* and Δ*mucR1/2 C. crescentus* cells.

A

MucR1/2 ⊣ G1 promoters

CtrA~P → G1 promoters

Cell cycle

SW (G1 promoters ON)

ST (G1 promoters OFF)

G1   S   G2/Division

B

MucR1/2 ⊣ m6A

CcrM → m6A

Chromosome replication

★ Origin of replication

▽ Terminus

● Replisome

— Hemi-methylated chromosome

= Fully methylated chromosome

T10   T40   T70   T100

A

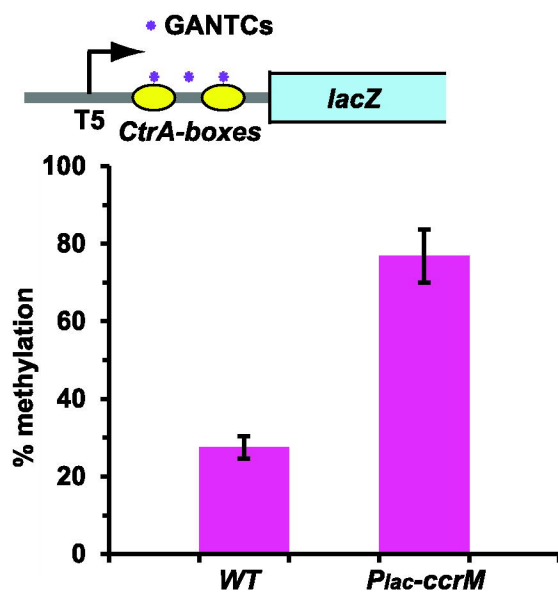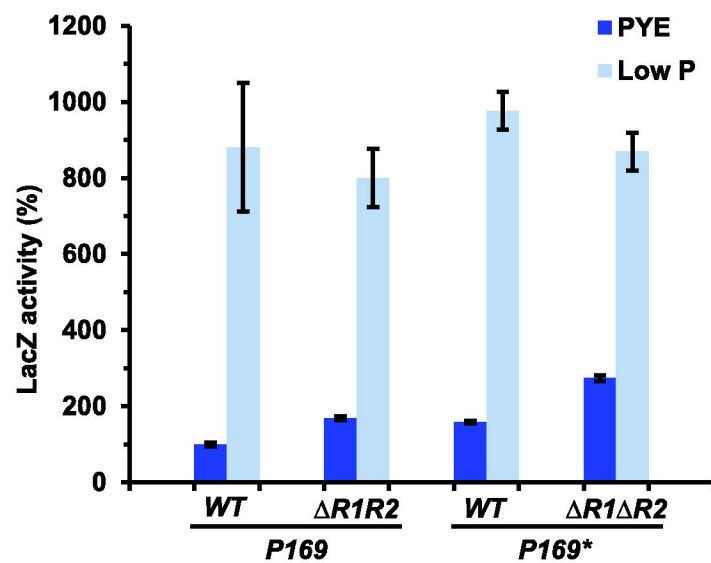MucR1 occupancy   * Unmethylated GANTC sites   Transcription start site   (⌐ sense; ⌐ anti-sense)

B

P169

P1149

1083

P2830

P2901

P3248
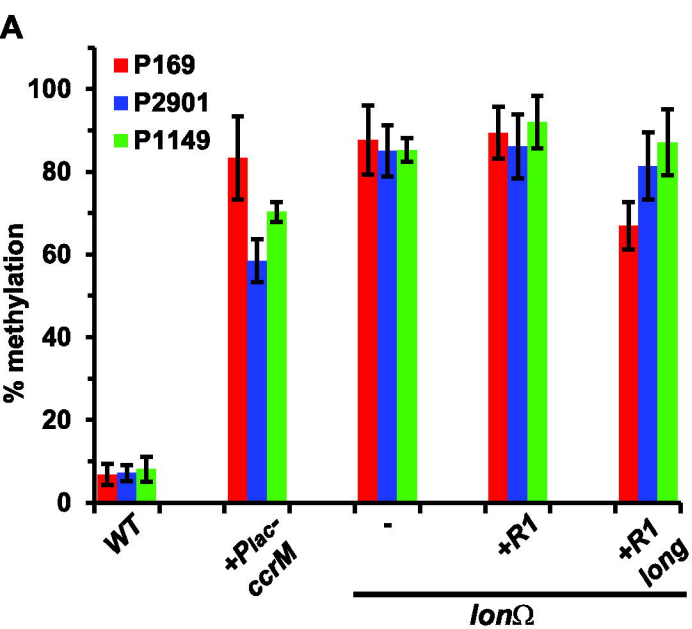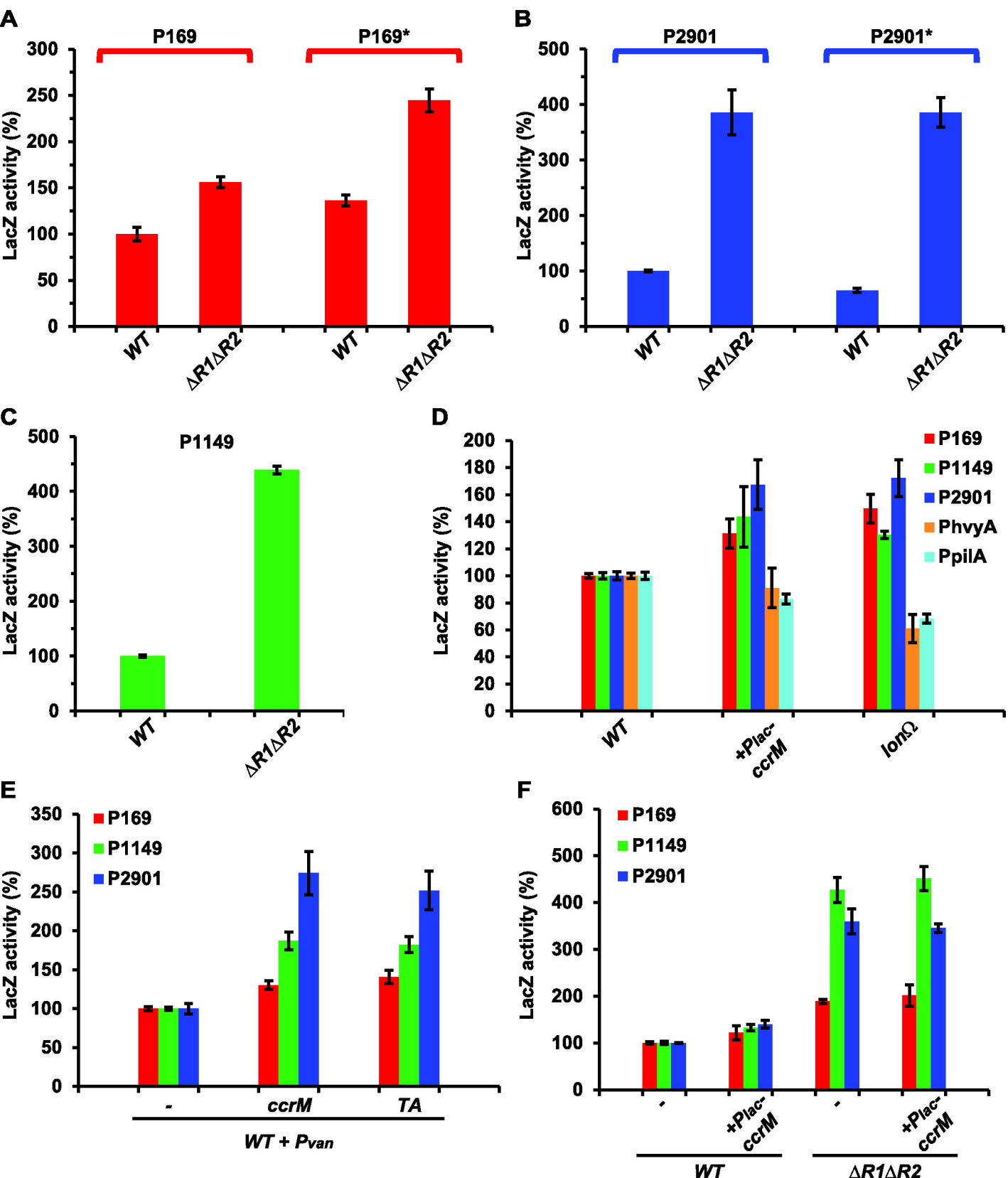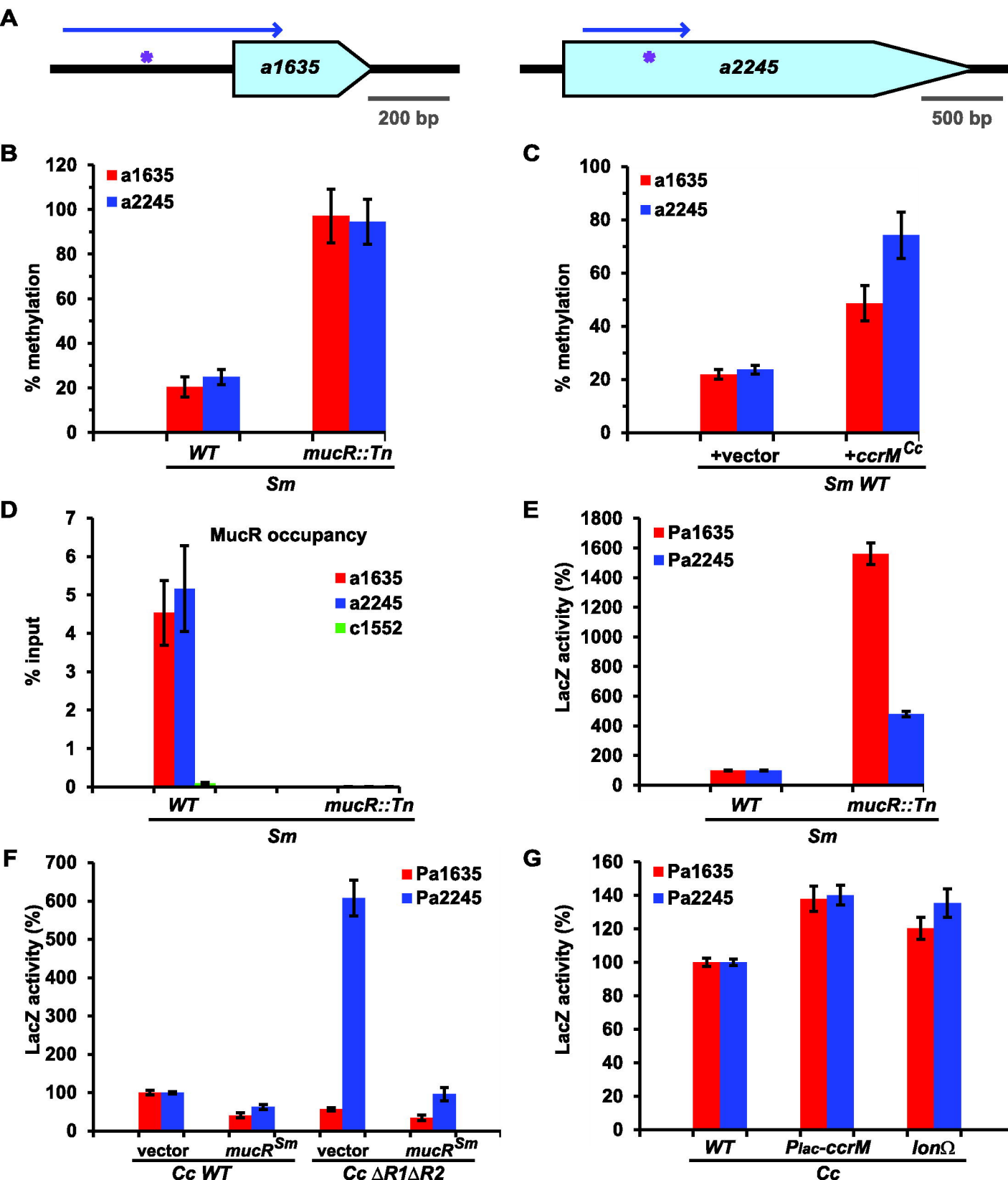
A CtrA vs CcrM competition